iScience, Volume *25*

Supplemental information

Shared and unique phosphoproteomics responses in skeletal muscle from exercise models and in hyperammonemic myotubes

Nicole Welch, Shashi Shekhar Singh, Ryan Musich, M. Shahid Mansuri, Annette Bellar, Saurabh Mishra, Aruna K. Chelluboyina, Jinendiran Sekar, Amy H. Attaway, Ling Li, Belinda Willard, Troy A. Hornberger, and Srinivasan Dasarathy

6hAmAc

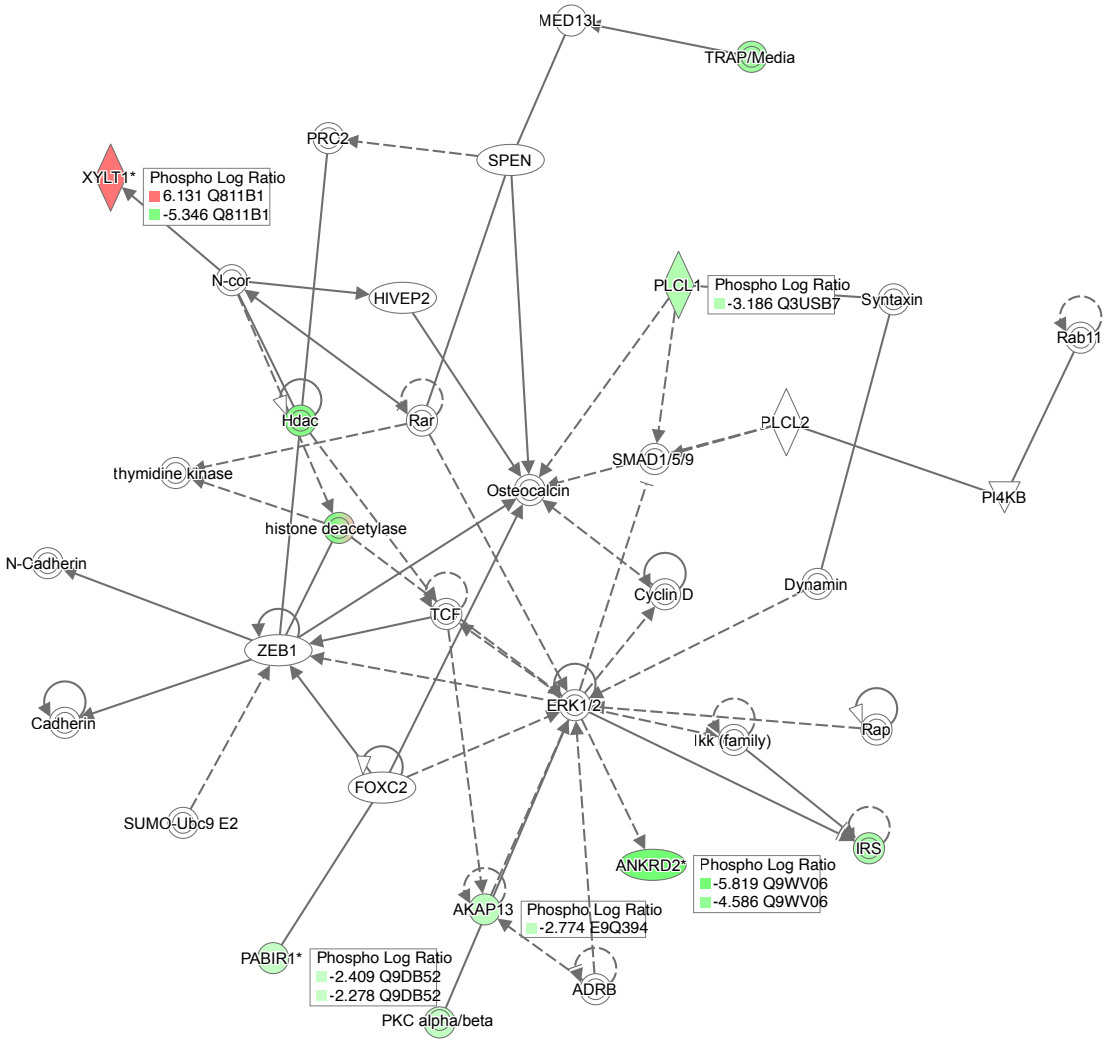

24hAmAc

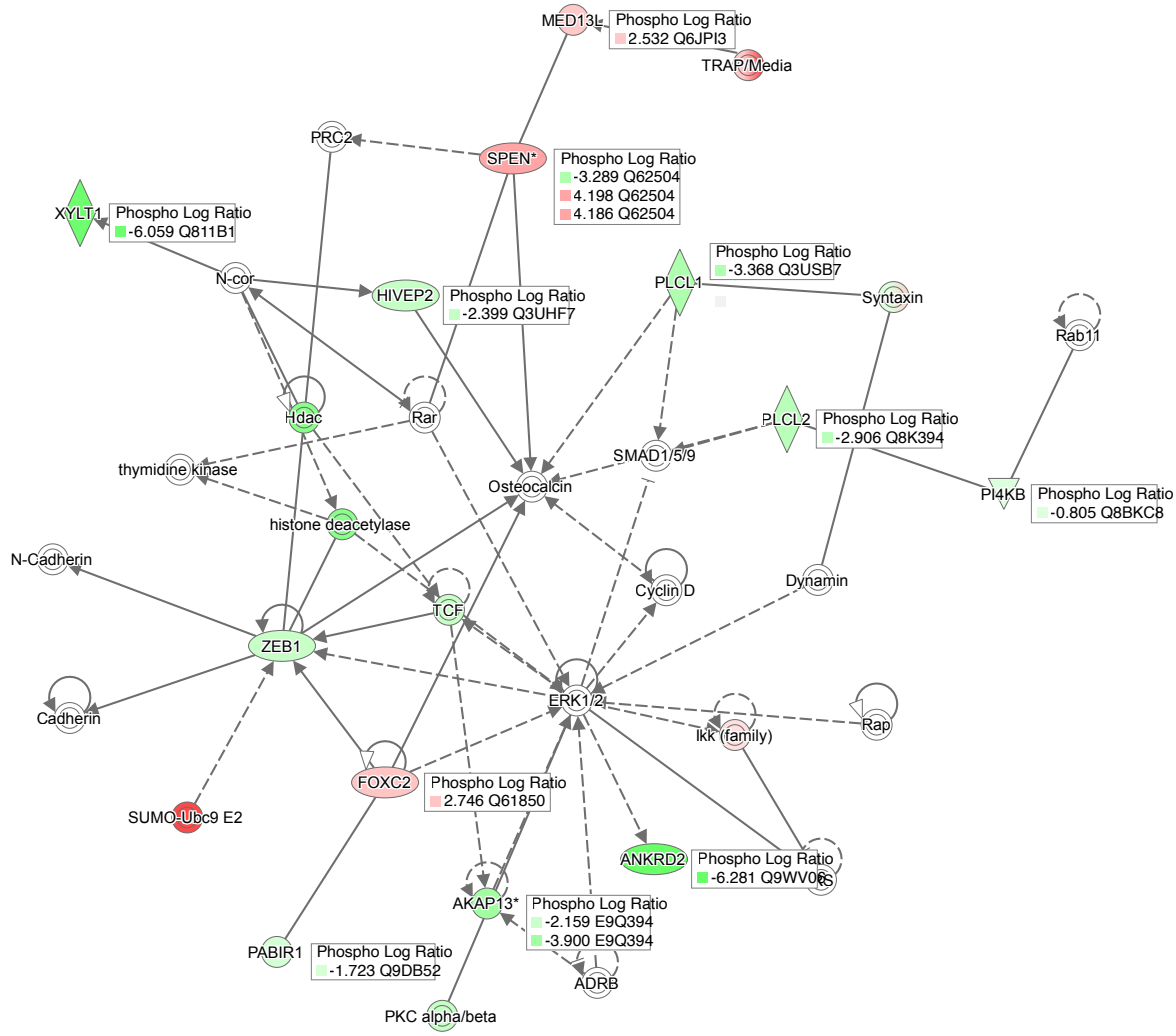

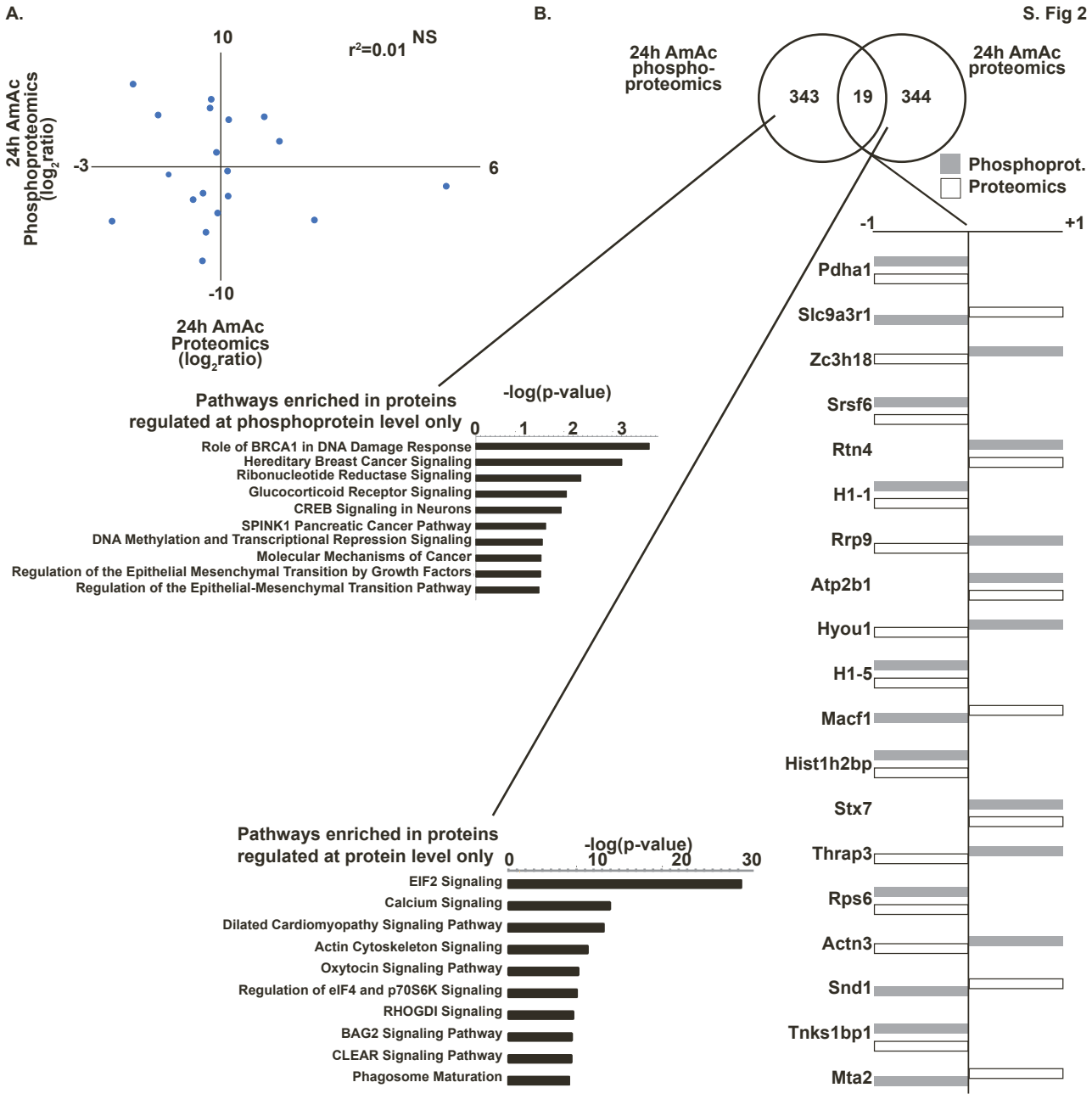
A.
B.
10
-10
-3
6
r²=0.01 NS
24h AmAc Phosphoproteomics (log2ratio)
24h AmAc Proteomics (log2ratio)
24h AmAc phospho-proteomics
24h AmAc proteomics
343
19
344
Phosphoprot.
Proteomics
-1
+1
Pdha1
Slc9a3r1
Zc3h18
Srsf6
Rtn4
H1-1
Rrp9
Atp2b1
Hyou1
H1-5
Macf1
Hist1h2bp
Stx7
Thrap3
Rps6
Actn3
Snd1
Tnks1bp1
Mta2
Pathways enriched in proteins regulated at phosphoprotein level only
-log(p-value)
0
1
2
3
Role of BRCA1 in DNA Damage Response
Hereditary Breast Cancer Signaling
Ribonucleotide Reductase Signaling
Glucocorticoid Receptor Signaling
CREB Signaling in Neurons
SPINK1 Pancreatic Cancer Pathway
DNA Methylation and Transcriptional Repression Signaling
Molecular Mechanisms of Cancer
Regulation of the Epithelial Mesenchymal Transition by Growth Factors
Regulation of the Epithelial-Mesenchymal Transition Pathway
Pathways enriched in proteins regulated at protein level only
-log(p-value)
0
10
20
30
EIF2 Signaling
Calcium Signaling
Dilated Cardiomyopathy Signaling Pathway
Actin Cytoskeleton Signaling
Oxytocin Signaling Pathway
Regulation of eIF4 and p70S6K Signaling
RHOGDI Signaling
BAG2 Signaling Pathway
CLEAR Signaling Pathway
Phagosome Maturation

A. 6hAmAc Unique DEpP

IPA canonical pathway enrichment

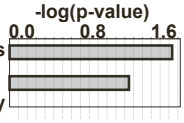

DAVID functional annotation	Enrichment scores
Cell projection/cytoskeleton	(2.24)
Zinc-ion binding	(1.35)
Microtubule	(1.18)
WD40 repeat	(0.66)
Pleckstrin homology domain	(0.64)

B. 24hAmAc Unique DEpP

IPA canonical pathway enrichment

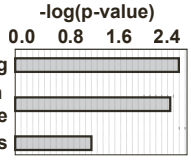

DAVID functional annotation Cluster 1

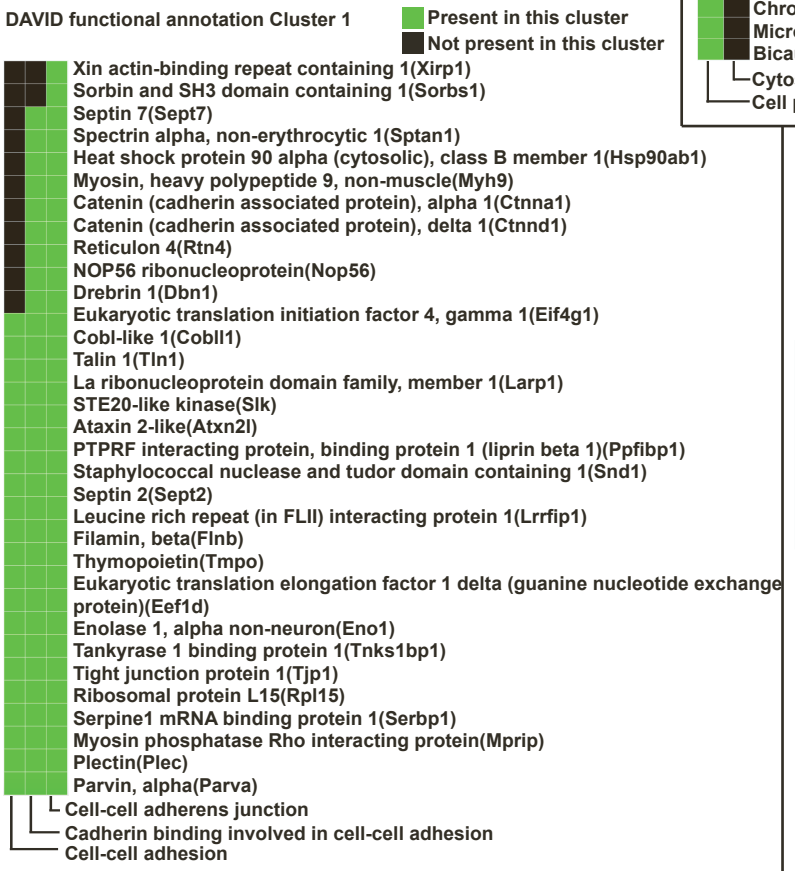

DAVID functional annotation	Enrichment scores
Cell-cell adhesion	(1.94)
Calmodulin-binding	(1.09)
G-protein coupled signaling	(0.80)
Zinc-ion binding	(0.76)
Protein serine/threonine/tyrosine kinase activity	(0.71)
Immunoglobulin-like domain	(0.69)
Pleckstrin homology domain	(0.62)
PWWP	(0.62)

DAVID functional annotation Cluster 1

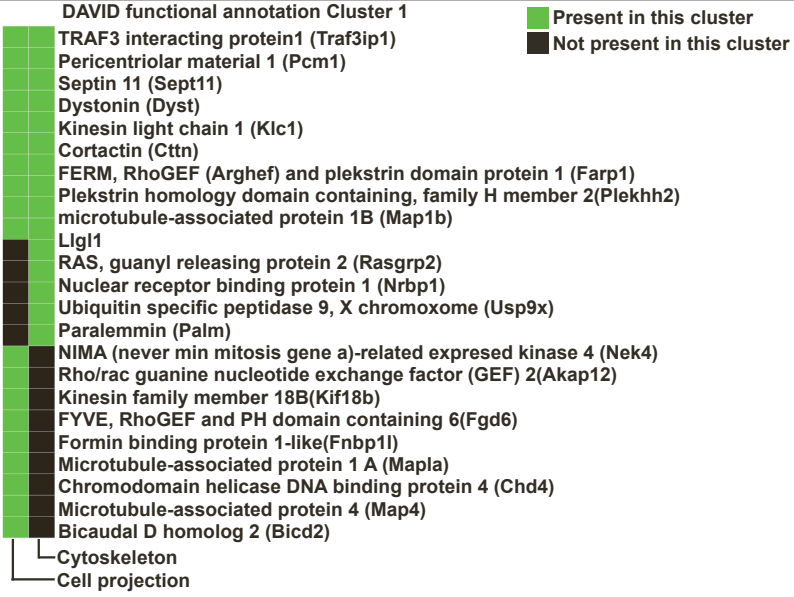

C. 6h and 24hAmAc Shared

IPA canonical pathway enrichment

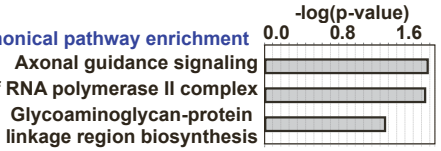

DAVID functional annotation Cluster 1

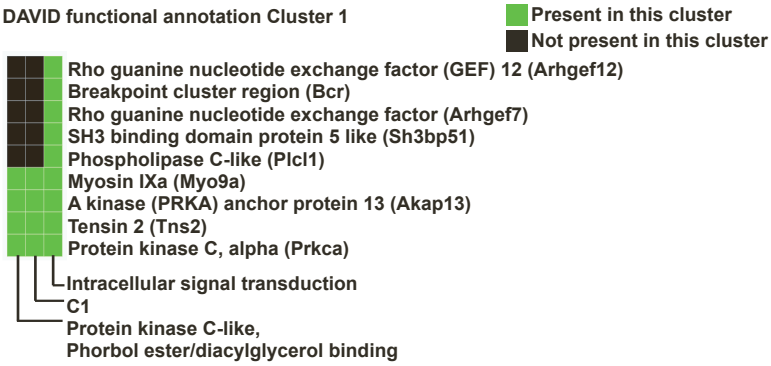

DAVID functional annotation	Enrichment scores
Protein kinase C-like phorbol ester/diacylglycerol binding	(1.70)
Pleckstrin homology domain/ intracellular signal transduction	(1.56)
SH3 domain	(1.21)
mRNA splicing	(1.01)
Ankyrin repeat-containing domain	(0.66)
C2 caldium-dependent membrane targeting	(0.64)
Cell differentiation	(0.62)
Rho GTPase activator activity	(0.60)

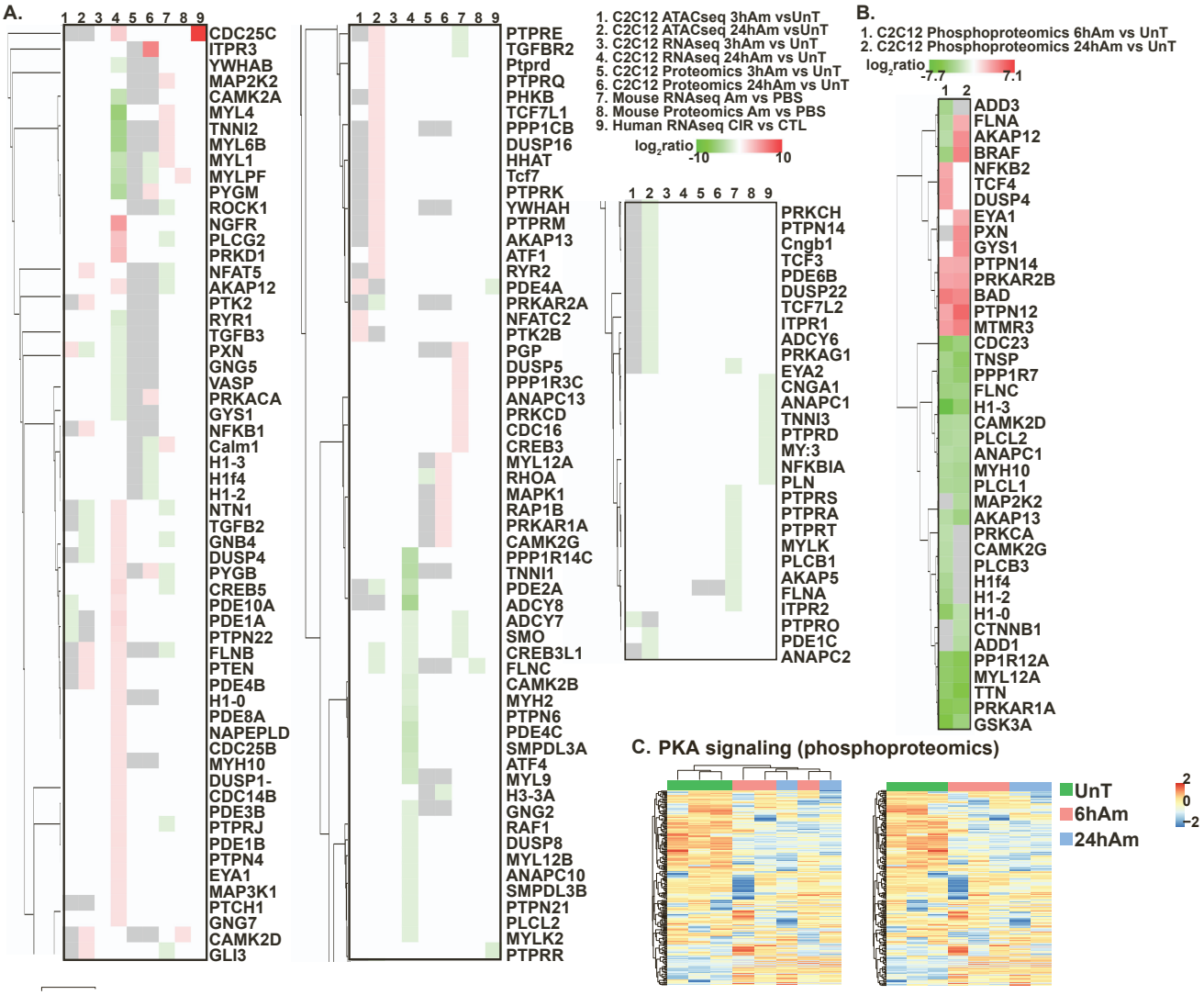
A.
1 2 3 4 5 6 7 8 9
CDC25C
ITPR3
YWHAB
MAP2K2
CAMK2A
MYL4
TNNI2
MYL6B
MYL1
MYLPF
PYGM
ROCK1
NGFR
PLCG2
PRKD1
NFAT5
AKAP12
PTK2
RYR1
TGFB3
PXN
GNG5
VASP
PRKACA
GYS1
NFKB1
Calm1
H1-3
H1f4
H1-2
NTN1
TGFB2
GNB4
DUSP4
PYGB
CREB5
PDE10A
PDE1A
PTPN22
FLNB
PTEN
PDE4B
H1-0
PDE8A
NAPEPLD
CDC25B
MYH10
DUSP1-
CDC14B
PDE3B
PTPRJ
PDE1B
PTPN4
EYA1
MAP3K1
PTCH1
GNG7
CAMK2D
GLI3
PTPRE
TGFBR2
Ptprd
PTPRQ
PHKB
TCF7L1
PPP1CB
DUSP16
HHAT
Tcf7
PTPRK
YWHAH
PTPRM
AKAP13
ATF1
RYR2
PDE4A
PRKAR2A
NFATC2
PTK2B
PGP
DUSP5
PPP1R3C
ANAPC13
PRKCD
CDC16
CREB3
MYL12A
RHOA
MAPK1
RAP1B
PRKAR1A
CAMK2G
PPP1R14C
TNNI1
PDE2A
ADCY8
ADCY7
SMO
CREB3L1
FLNC
CAMK2B
MYH2
PTPN6
PDE4C
SMPDL3A
ATF4
MYL9
H3-3A
GNG2
RAF1
DUSP8
MYL12B
ANAPC10
SMPDL3B
PTPN21
PLCL2
MYLK2
PTPRR
1. C2C12 ATACseq 3hAm vsUnT
2. C2C12 ATACseq 24hAm vsUnT
3. C2C12 RNAseq 3hAm vs UnT
4. C2C12 RNAseq 24hAm vs UnT
5. C2C12 Proteomics 3hAm vs UnT
6. C2C12 Proteomics 24hAm vs UnT
7. Mouse RNAseq Am vs PBS
8. Mouse Proteomics Am vs PBS
9. Human RNAseq CIR vs CTL
log2ratio
-10
10
1 2 3 4 5 6 7 8 9
PRKCH
PTPN14
Cngb1
TCF3
PDE6B
DUSP22
TCF7L2
ITPR1
ADCY6
PRKAG1
EYA2
CNGA1
ANAPC1
TNNI3
PTPRD
MY:3
NFKBIA
PLN
PTPRS
PTPRA
PTPRT
MYLK
PLCB1
AKAP5
FLNA
ITPR2
PTPRO
PDE1C
ANAPC2
B.
1. C2C12 Phosphoproteomics 6hAm vs UnT
2. C2C12 Phosphoproteomics 24hAm vs UnT
log2ratio
-7.7
7.1
1 2
ADD3
FLNA
AKAP12
BRAF
NFKB2
TCF4
DUSP4
EYA1
PXN
GYS1
PTPN14
PRKAR2B
BAD
PTPN12
MTMR3
CDC23
TNSP
PPP1R7
FLNC
H1-3
CAMK2D
PLCL2
ANAPC1
MYH10
PLCL1
MAP2K2
AKAP13
PRKCA
CAMK2G
PLCB3
H1f4
H1-2
H1-0
CTNNB1
ADD1
PP1R12A
MYL12A
TTN
PRKAR1A
GSK3A
C. PKA signaling (phosphoproteomics)
UnT
6hAm
24hAm
2
0
−2

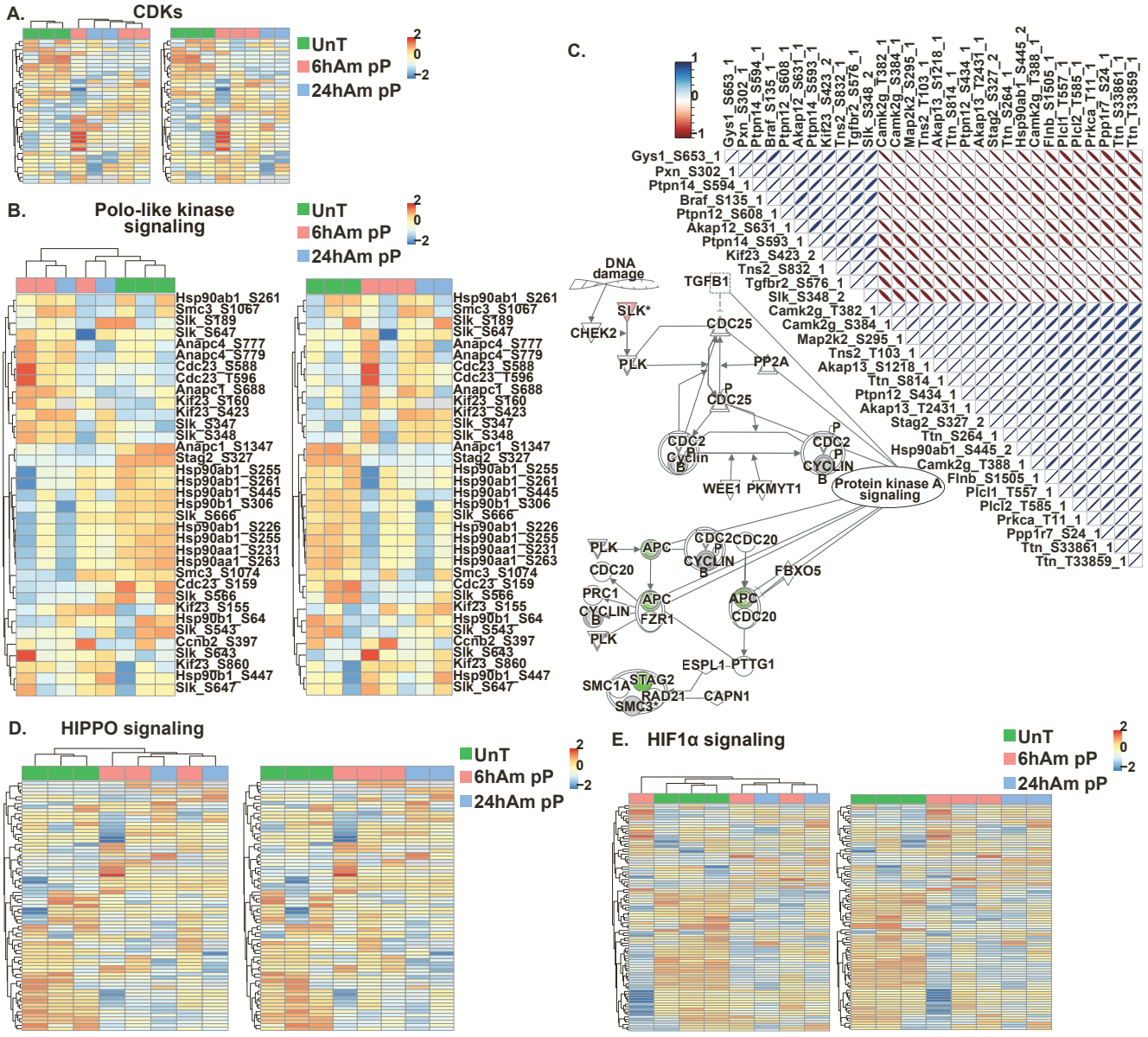
A.
CDKs
UnT
6hAm pP
24hAm pP
B.
Polo-like kinase signaling
Hsp90ab1_S261
Smc3_S1067
Slk_S189
Slk_S647
Anapc4_S777
Anapc4_S779
Cdc23_S588
Cdc23_T596
Anapc1_S688
Kif23_S160
Kif23_S423
Slk_S347
Slk_S348
Anapc1_S1347
Stag2_S327
Hsp90ab1_S255
Hsp90ab1_S261
Hsp90ab1_S445
Hsp90b1_S306
Slk_S666
Hsp90ab1_S226
Hsp90ab1_S255
Hsp90aa1_S231
Hsp90aa1_S263
Smc3_S1074
Cdc23_S159
Slk_S566
Kif23_S155
Hsp90b1_S64
Slk_S543
Ccnb2_S397
Slk_S643
Kif23_S860
Hsp90b1_S447
Slk_S647
C.
DNA damage
TGFB1
SLK*
CHEK2
CDC25
PLK
PP2A
P
CDC25
CDC2
Cyclin
B
CDC2
P
CYCLIN
B
WEE1
PKMYT1
Protein kinase A signaling
PLK
APC
CDC2
P
CDC20
CYCLIN
B
CDC20
FBXO5
PRC1
CYCLIN
B
APC
FZR1
APC
CDC20
PLK
ESPL1
PTTG1
SMC1A
STAG2
RAD21
SMC3
CAPN1
D.
HIPPO signaling
E.
HIF1α signaling

S.Fig 6

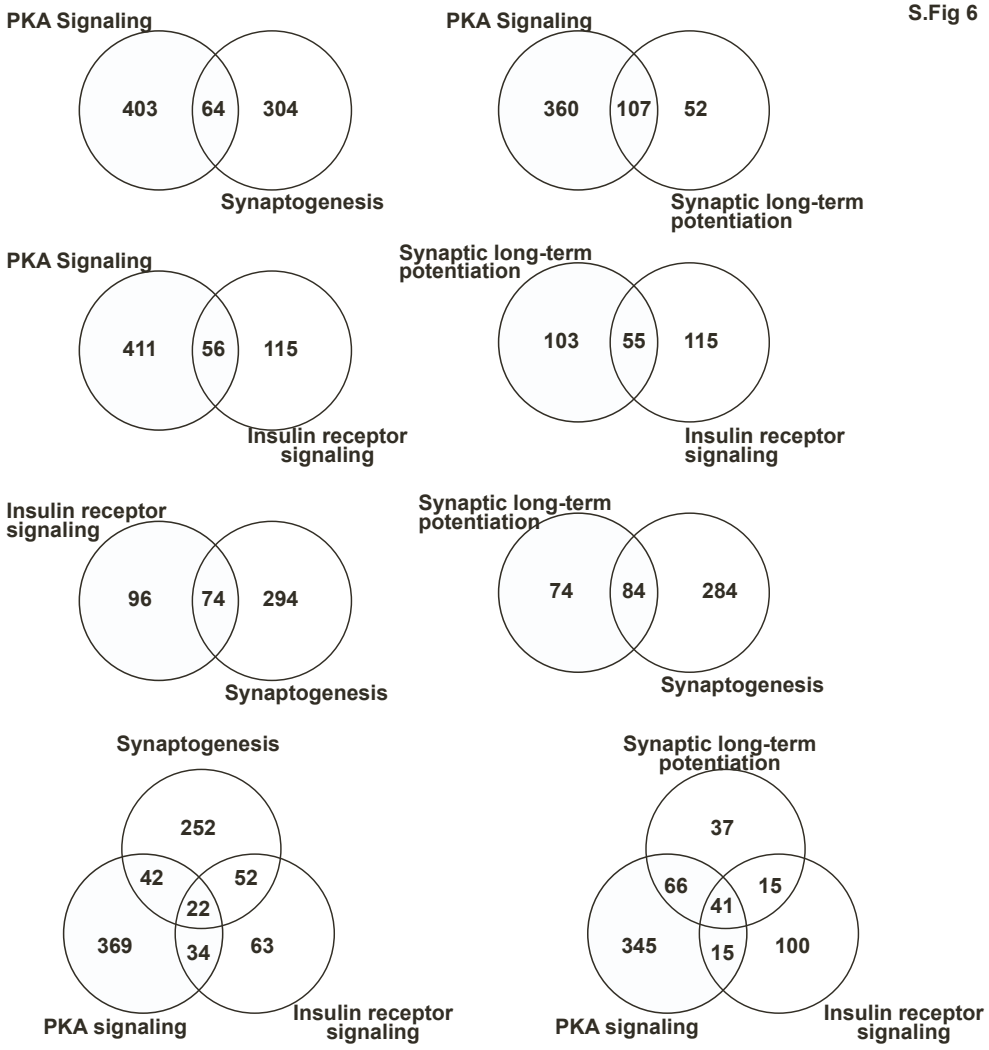
PKA Signaling
403
64
304
Synaptogenesis
PKA Signaling
360
107
52
Synaptic long-term potentiation
PKA Signaling
411
56
115
Insulin receptor signaling
Synaptic long-term potentiation
103
55
115
Insulin receptor signaling
Insulin receptor signaling
96
74
294
Synaptogenesis
Synaptic long-term potentiation
74
84
284
Synaptogenesis
Synaptogenesis
252
42
52
22
369
34
63
PKA signaling
Insulin receptor signaling
Synaptic long-term potentiation
37
66
15
41
345
15
100
PKA signaling
Insulin receptor signaling

A. Cluster 1. Persistent increase

Category	Term
UP:Keywords	Synapse
UP:Keywords	Transcription
UP:Keywords	Cell junction
UP:Keywords	Transcription regulation
KEGG Pathway	mmu04510:Focal adhesion
GO:MF	GO:0001077~transcriptional activator activity, RNA polymerase II core
GO:BP	promoter proximal region sequence-specific binding
GO:CC	GO:0008285~regulation of cell proliferation
GO:BP	GO:0030054~cell junction
GO:MF	GO:0007026~regulation of microtubule depolymerization
GO:BP	GO:0042826~histone deacetylase binding
GO:BP	GO:0006351~transcription, DNA-templated
GO:CC	GO:0030155~regulation of cell adhesion
GO:BP	GO:0043197~dendritic spine
GO:BP	GO:0030900~forebrain development
KEGG Pathway	GO:0006355~regulation of transcription, DNA-templated
UP:Keywords	mmu04810:Regulation of actin cytoskeleton
GO:MF	Guanine-nucleotide releasing factor
KEGG Pathway	GO:0003677~DNA binding
UP:Seq Feature	mmu04022:cGMP-PKG signaling pathway repeat:3
UP:Keywords	Synaptosome
UP:Seq Feature	zinc finger region:Phorbol-ester/DAG-type Repressor repeat:1

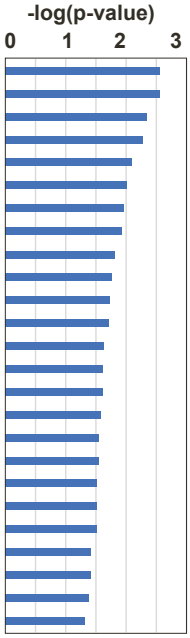

B. Cluster 2. Late increase

Category	Term
UP:Seq Feature	Compositionally biased region: Pro-rich
GO:BP	Response to food

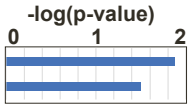

C. Cluster 3. Late decrease

Category	Term
UP:Keywords	Acetylation
GO:BP	GO:0098609~cell-cell adhesion
UP:Seq Features	short sequence motif:Nuclear localization signal
GO:CC	GO:0005913~cell-cell adherens junction
GO:MF	GO:0098641~cadherin binding involved in cell-cell adhesion
GO:BP	GO:0035264~multicellular organism growth
UP:Keywords	Citrullination
GO:CC	GO:0005737~cytoplasm
GO:MF	GO:0044822~poly(A) RNA binding
GO:MF	GO:0003779~actin binding
UP:Keywords	Chromosome

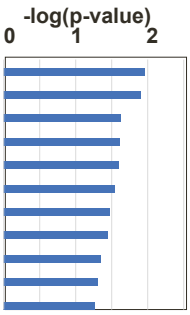

D. Cluster 4. Transient change

Category	Term
GO:MF	protein binding
GO:MF	protein domain specific binding
GO:BP	regulation of transcription, DNA-templated

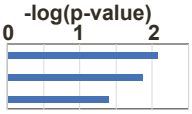

E. Cluster 5. Persistent decrease

Category	Term
UP:Seq Feature	compositionally biased region:Pro-rich
UP:Keywords	SH3 domain
GO:MF	GO:0098641~cadherin binding involved in cell-cell adhesion
Interpro	IPR001452:Src homology-3 domain
GO:CC	GO:0005913~cell-cell adherens junction
Interpro	IPR019787:Zinc finger, PHD-finger
GO:CC	GO:0030426~growth cone
Interpro	IPR001965:Zinc finger, PHD-type
UP:Keywords	Cell junction
SMART	SM00326:SH3
GO:MF	GO:0051015~actin filament binding
SMART	SM00249:PHD
UP:Keywords	Actin-binding
UP:Seq Feature	compositionally biased region:Ser-rich
GO:CC	GO:0005886~plasma membrane
GO:CC	GO:0031674~I band
UP:Keywords	Alternative promoter usage
GO:CC	GO:0005622~intracellular
UP:Seq Feature	zinc finger region:PHD-type
GO:MF	GO:0003779~actin binding
GO:CC	GO:0043197~dendritic spine
GO:CC	GO:0030054~cell junction
Interpro	IPR019786:Zinc finger, PHD-type, conserved site
Interpro	IPR011011:Zinc finger, FYVE/PHD-type
GO:CC	GO:0042995~cell projection
GO:MF	GO:0005516~calmodulin binding
GO:CC	GO:0043005~neuron projection
UP:Keywords	Cell projection
GO:BP	GO:0035556~intracellular signal transduction
UP:Keywords	Calcium

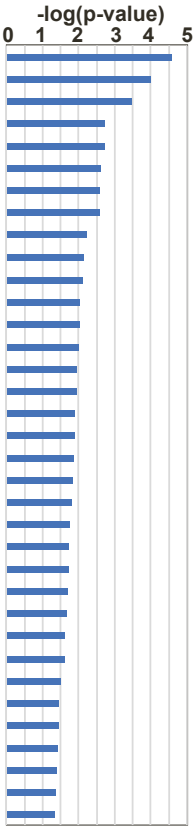

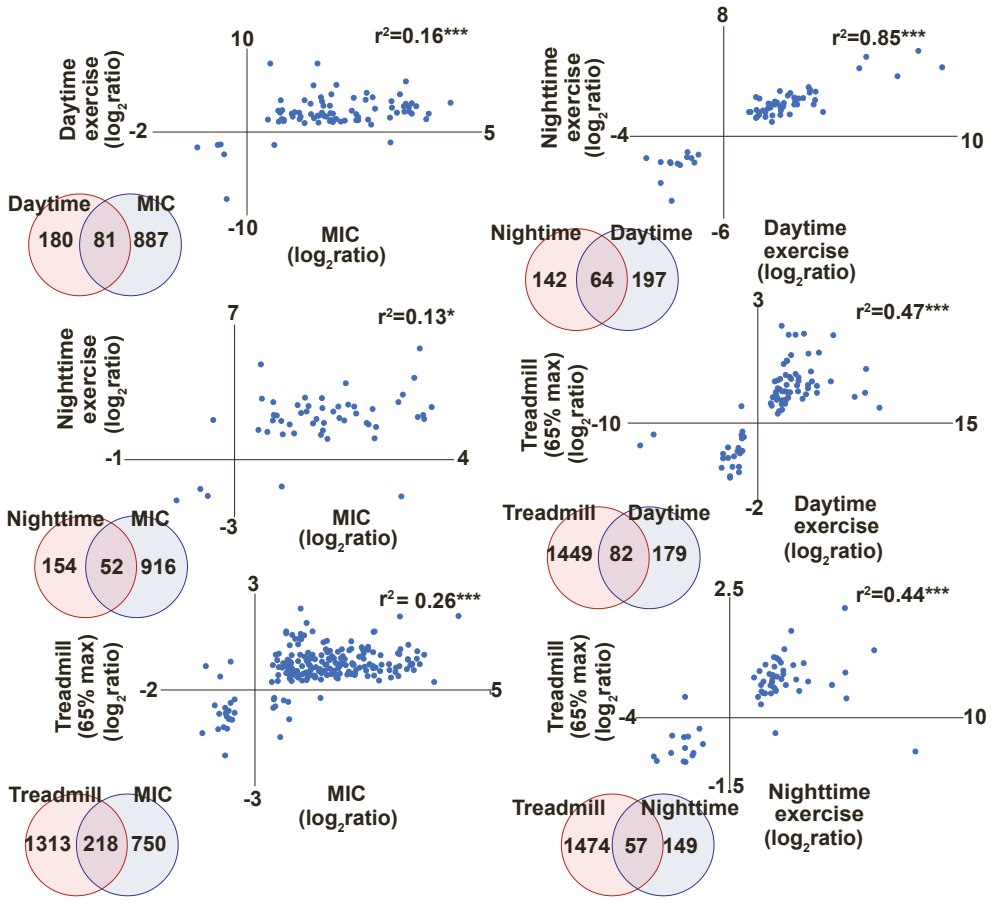
r²=0.16***
Daytime exercise (log2 ratio)
MIC (log2 ratio)
10
-10
-2
5
Daytime
MIC
180
81
887
r²=0.85***
Nighttime exercise (log2 ratio)
Daytime exercise (log2 ratio)
8
-6
-4
10
Nighttime
Daytime
142
64
197
r²=0.13*
Nighttime exercise (log2 ratio)
MIC (log2 ratio)
7
-3
-1
4
Nighttime
MIC
154
52
916
r²=0.47***
Treadmill (65% max) (log2 ratio)
Daytime exercise (log2 ratio)
3
-2
-10
15
Treadmill
Daytime
1449
82
179
r²= 0.26***
Treadmill (65% max) (log2 ratio)
MIC (log2 ratio)
3
-3
-2
5
Treadmill
MIC
1313
218
750
r²=0.44***
Treadmill (65% max) (log2 ratio)
Nighttime exercise (log2 ratio)
2.5
-1.5
-4
10
Treadmill
Nighttime
1474
57
149

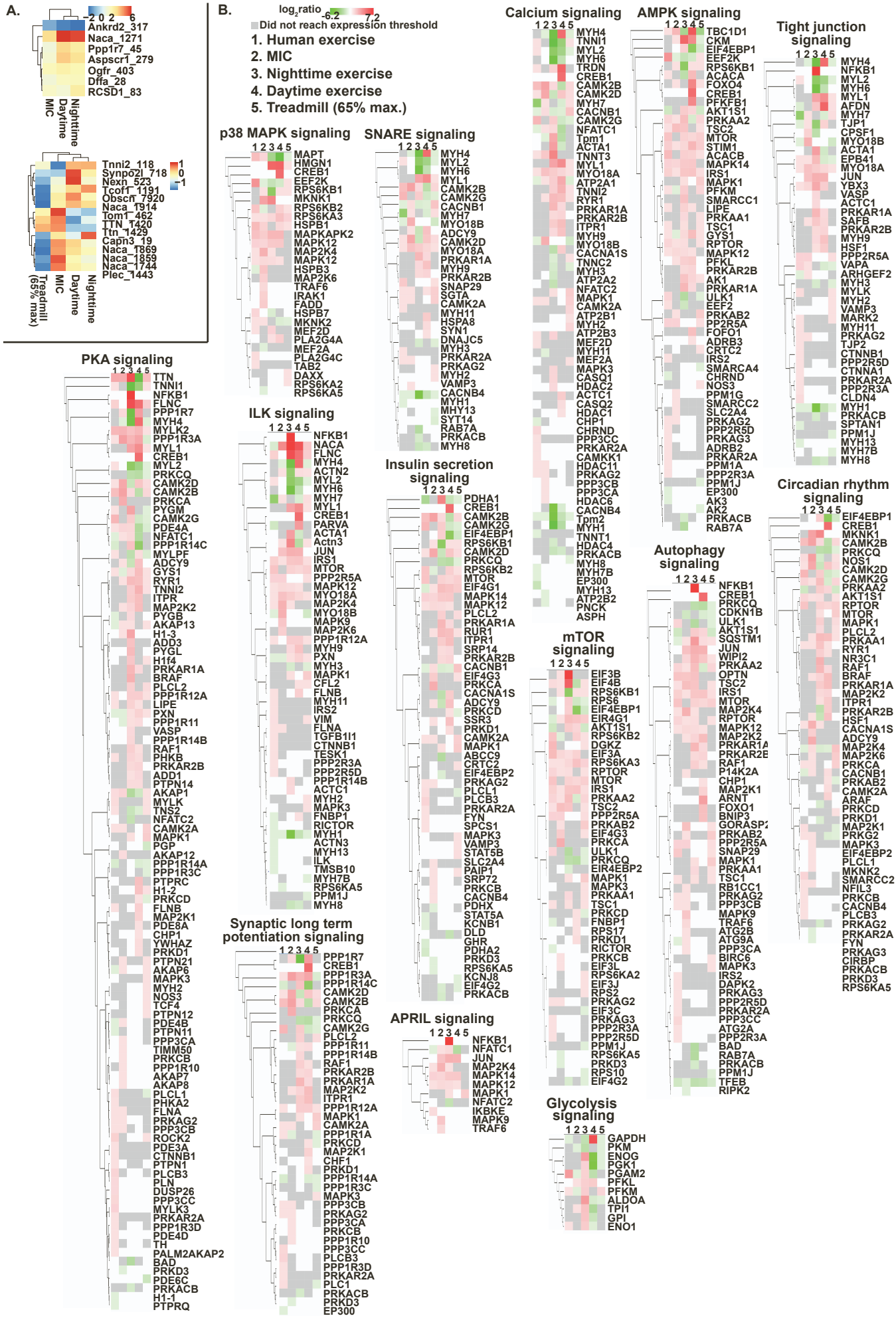
A.
Ankrd2_317
Naca_1271
Ppp1r7_45
Aspscr1_279
Ogfr_403
Dffa_28
RCSD1_83
MIC
Daytime
Nighttime
Tnni2_118
Synpo2l_718
Nexn_523
Tcof1_1191
Obscn_7920
Naca_1914
Tom1_462
TTN_1420
Ttn_1429
Capn3_19
Naca_1869
Naca_1859
Naca_1744
Plec_1443
Treadmill (65% max)
B.
log2ratio -6.2 7.2
Did not reach expression threshold
1. Human exercise
2. MIC
3. Nighttime exercise
4. Daytime exercise
5. Treadmill (65% max.)
p38 MAPK signaling
SNARE signaling
Calcium signaling
AMPK signaling
Tight junction signaling
PKA signaling
ILK signaling
Insulin secretion signaling
Autophagy signaling
Circadian rhythm signaling
mTOR signaling
Synaptic long term potentiation signaling
APRIL signaling
Glycolysis signaling

S.Fig 10

A. AKAP

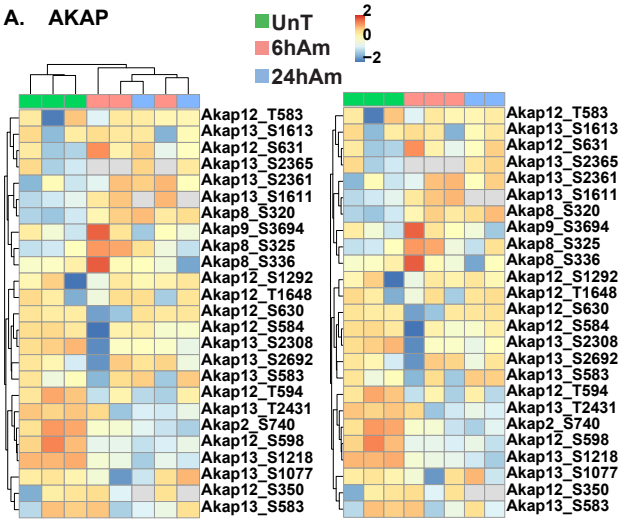

B.

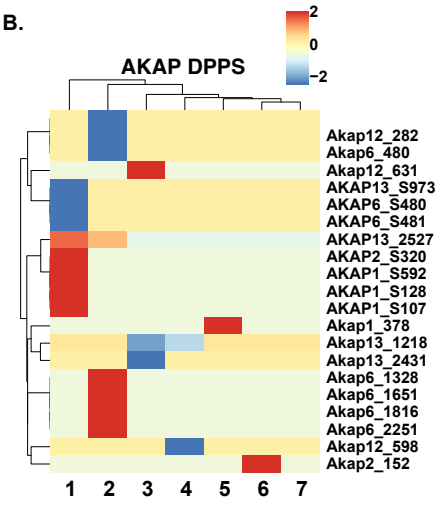

1. Human
2. Treadmill (65% max.)
3. 24h AmAc
4. 6h AmAc
5. MIC
6. Daytime exercise
7. Nighttime exercise

C. Enriched pathways in DEpP shared in AmAc and exercise (by model)

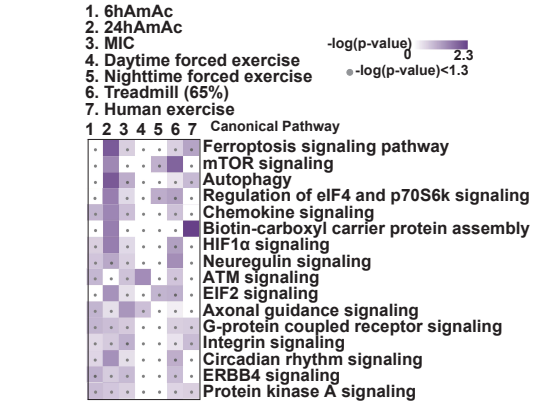

D. DEpP by AmAc dataset shared with exercise (24hAmAc representatitve)

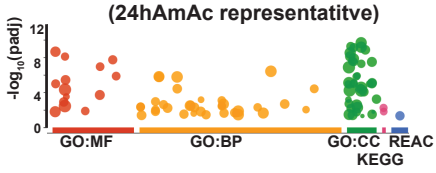

6hAmAc shared with exercise

RNA binding
Cytoskeletal protein binding
Tubulin binding
Enzyme binding
Protein binding
Guanyl-nucleotide exchange factor activity
RNA splicing
mRNA processing
mRNA splicing
mRNA transport
RNA processing
mRNA metabolic process
Establishment of RNA localization
Cell death signaling via NRAGE, NRIF, and NADE

24hAmAc shared with exercise

RNA binding
Calmodulin binding
Cytoskeletal binding
Actin binding
Structural constituent of muscle
Cadherin binding
Cell adhesion molecule binding
HIF1α signaling

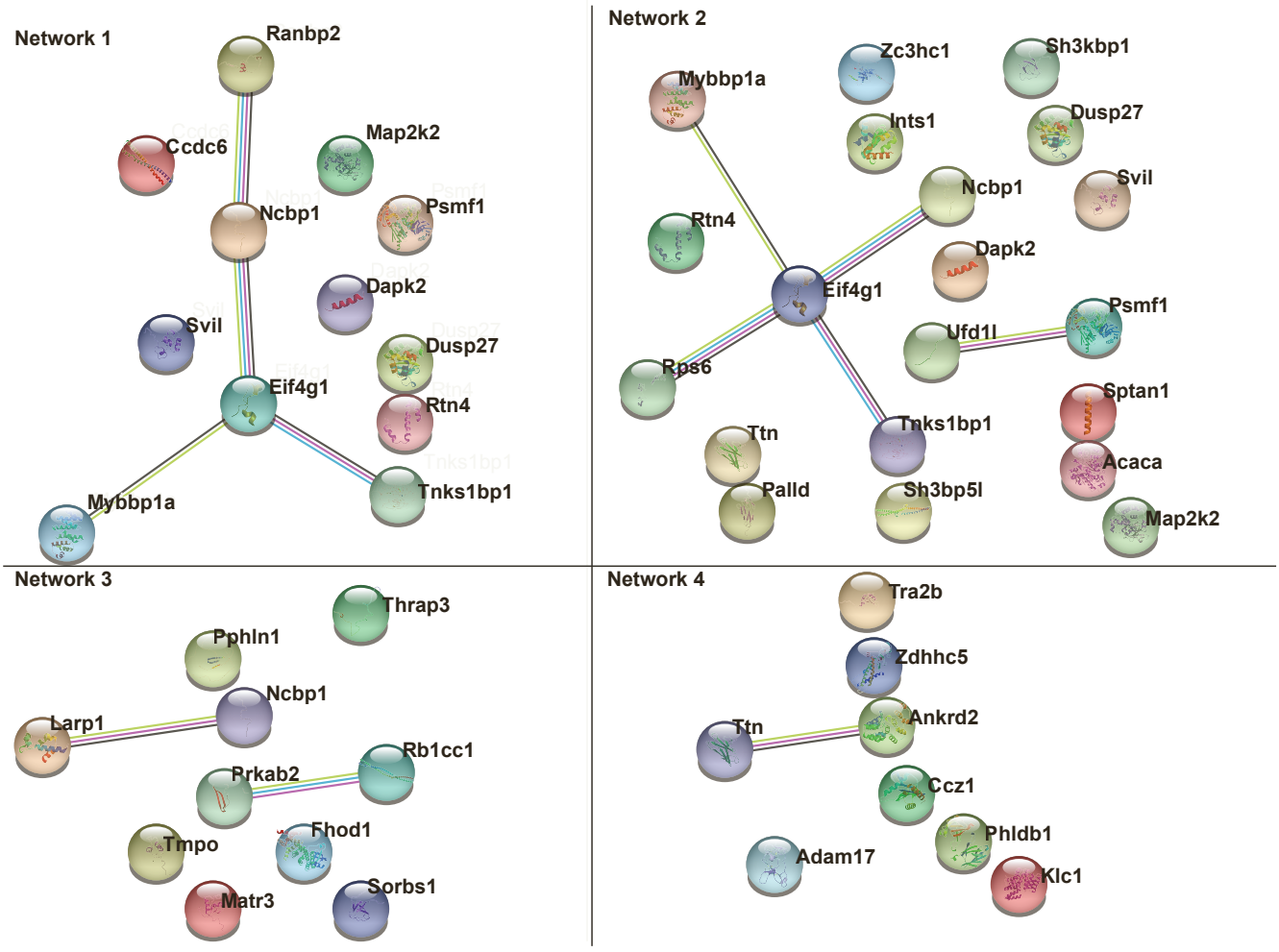
Network 1
Ranbp2
Ccdc6
Map2k2
Ncbp1
Psmf1
Dapk2
Svil
Dusp27
Eif4g1
Rtn4
Tnks1bp1
Mybbp1a
Network 2
Zc3hc1
Sh3kbp1
Mybbp1a
Ints1
Dusp27
Ncbp1
Svil
Rtn4
Dapk2
Eif4g1
Psmf1
Ufd1l
Rps6
Sptan1
Ttn
Tnks1bp1
Acaca
Palld
Sh3bp5l
Map2k2
Network 3
Thrap3
Pphln1
Ncbp1
Larp1
Rb1cc1
Prkab2
Fhod1
Tmpo
Sorbs1
Matr3
Network 4
Tra2b
Zdhhc5
Ttn
Ankrd2
Ccz1
Phldb1
Adam17
Klc1

S.Fig 12

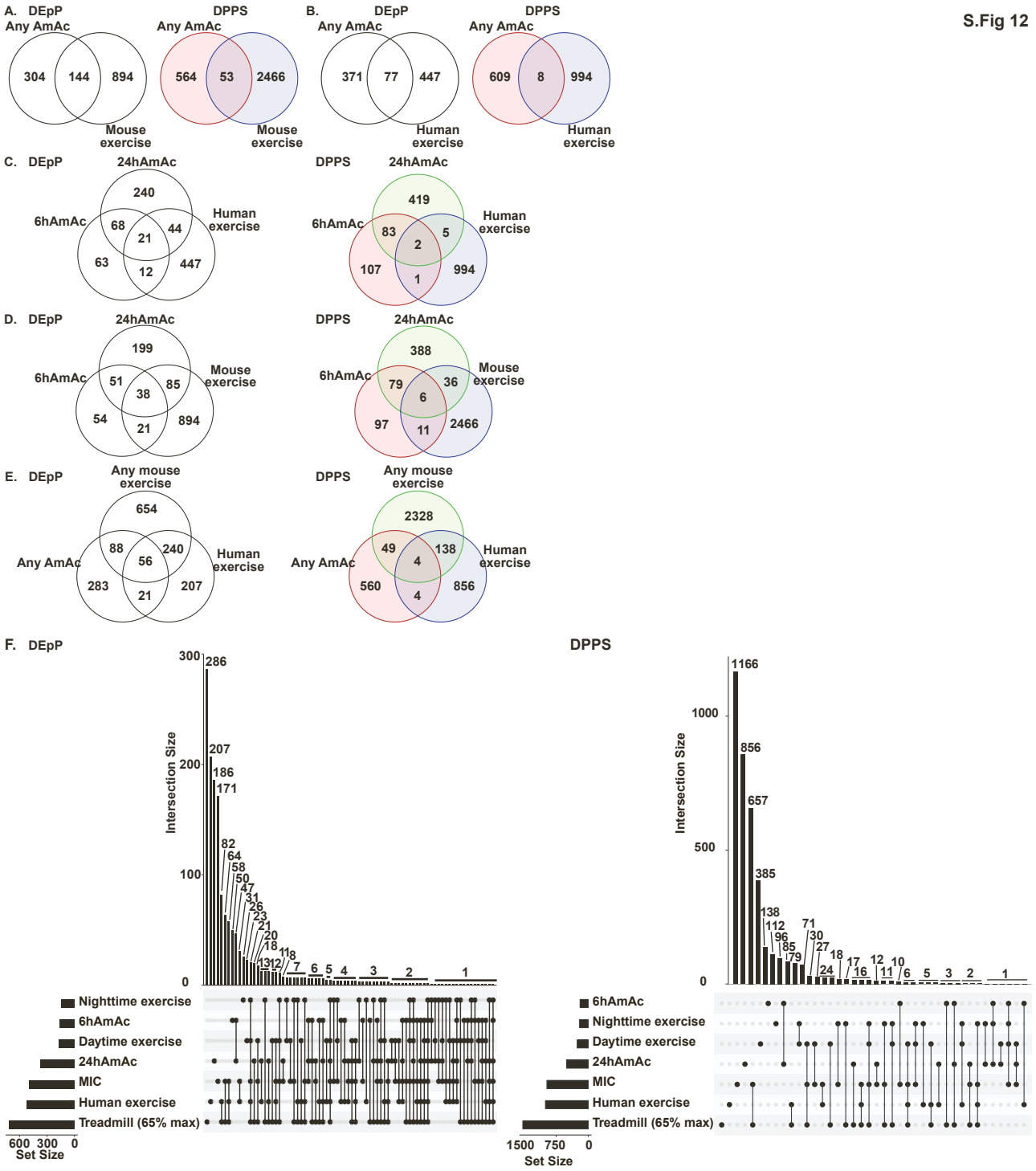
A. DEpP
Any AmAc
304
144
894
Mouse exercise
DPPS
Any AmAc
564
53
2466
Mouse exercise
B. DEpP
Any AmAc
371
77
447
Human exercise
DPPS
Any AmAc
609
8
994
Human exercise
C. DEpP
24hAmAc
240
6hAmAc
68
44
Human exercise
21
63
12
447
DPPS
24hAmAc
419
6hAmAc
83
5
Human exercise
2
107
1
994
D. DEpP
24hAmAc
199
6hAmAc
51
85
Mouse exercise
38
54
21
894
DPPS
24hAmAc
388
6hAmAc
79
36
Mouse exercise
6
97
11
2466
E. DEpP
Any mouse exercise
654
Any AmAc
88
240
Human exercise
56
283
21
207
DPPS
Any mouse exercise
2328
Any AmAc
49
138
Human exercise
4
560
4
856
F. DEpP
Intersection Size
300
200
100
0
286
207
186
171
82
64
58
50
47
31
26
23
21
20
18
11
8
13
12
7
6
5
4
3
2
1
Nighttime exercise
6hAmAc
Daytime exercise
24hAmAc
MIC
Human exercise
Treadmill (65% max)
600 300 0
Set Size
DPPS
Intersection Size
1000
500
0
1166
856
657
385
138
112
96
85
79
71
30
27
18
24
17
16
12
11
10
6
5
3
2
1
6hAmAc
Nighttime exercise
Daytime exercise
24hAmAc
MIC
Human exercise
Treadmill (65% max)
1500 750 0
Set Size

S.Fig 13

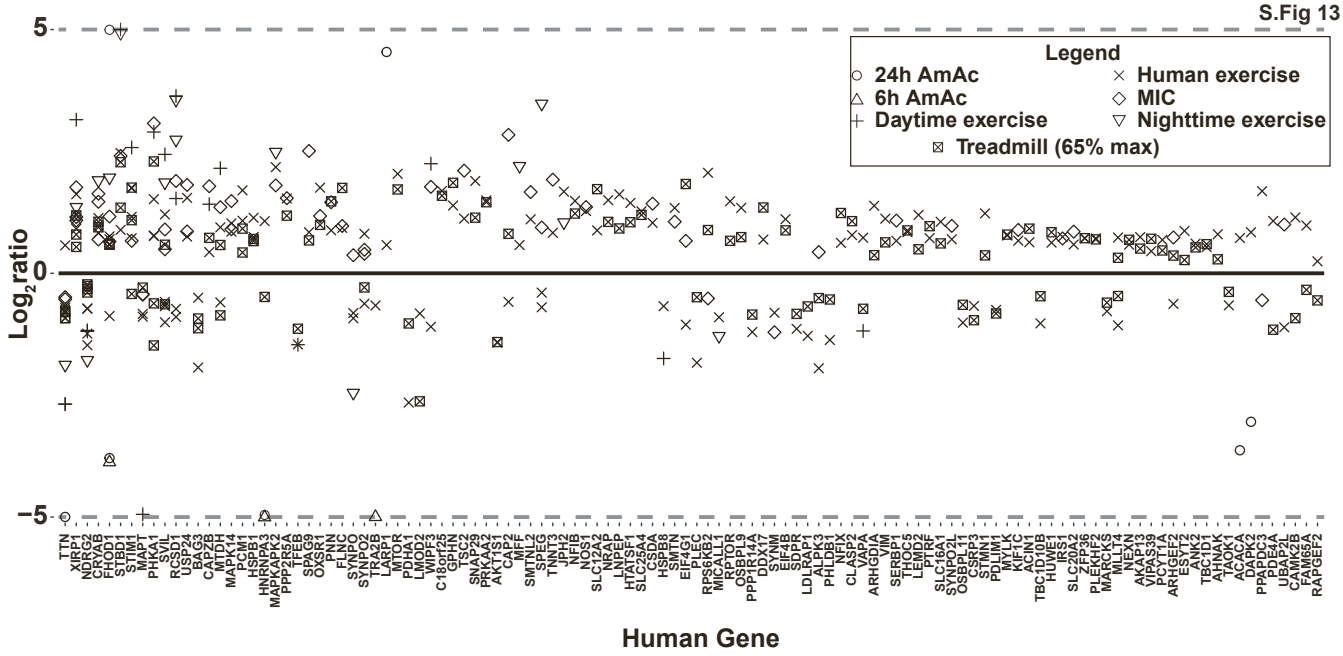
5
0
−5
Log2 ratio
Legend
24h AmAc
6h AmAc
Daytime exercise
Human exercise
MIC
Nighttime exercise
Treadmill (65% max)
TTN
XIRP1
NDRG2
CRYAB
FHOD1
STBD1
STIM1
MAPT
PHKA1
SSU1
RCSD1
USP24
BAG3
CAMTA1
ATP2B
MAPK14
PCM1
HSPB1
HNRNPA2
MAPKAPK2
PPP2R5A
TFEB
SPAG9
OXSR1
PPM1
FLNC
SYNPO2
STRBP
TRIP4
LARP1
MTOR
PDHA1
LMOD2
WIPF3
C18orf25
GPHN
TSC2
SNAP29
PRKAG2
AKT1S1
CAP2
MFF
SMTNL2
SPEG
TNNT3
JPH2
NFIB
NOS1
SLC12A2
NRAP
LNPEP
HTATSF1
SLC25A4
CSDA
HSPB8
SMTN
EIF4G1
PLEC
RPS6KB2
MICALL1
RPTOR
PPP3R1
PPP3CA
DDX17
SYNM
EIF4B
RDH11
LDLRAP1
ALPK3
PHLDB1
NFIX
CLASP2
VASP
ARHGDIA
VIM
SERBP1
THOC5
LEMD2
PTRF
SLC16A1
SYNPO2L
OSBPL11
CSRP3
STMN1
PDLIM1
MYLK
KIF1C
ACIN1
TBC1D10B
HUWE1
IRS1
SLC2A4
ZFP36
PLEKHF2
MARCKS
MLLT4
NEXN
AKAP13
VIPAS39
PCYT1A
ARGEF12
ESYT2
ANK2
TBC1D1
AHNAK
ZAK1
ACACA
DAPK2
PPAPDC3
DAB2IP
UBE2J1
CAMK2B
FAM65A
RAPGEF2
Human Gene

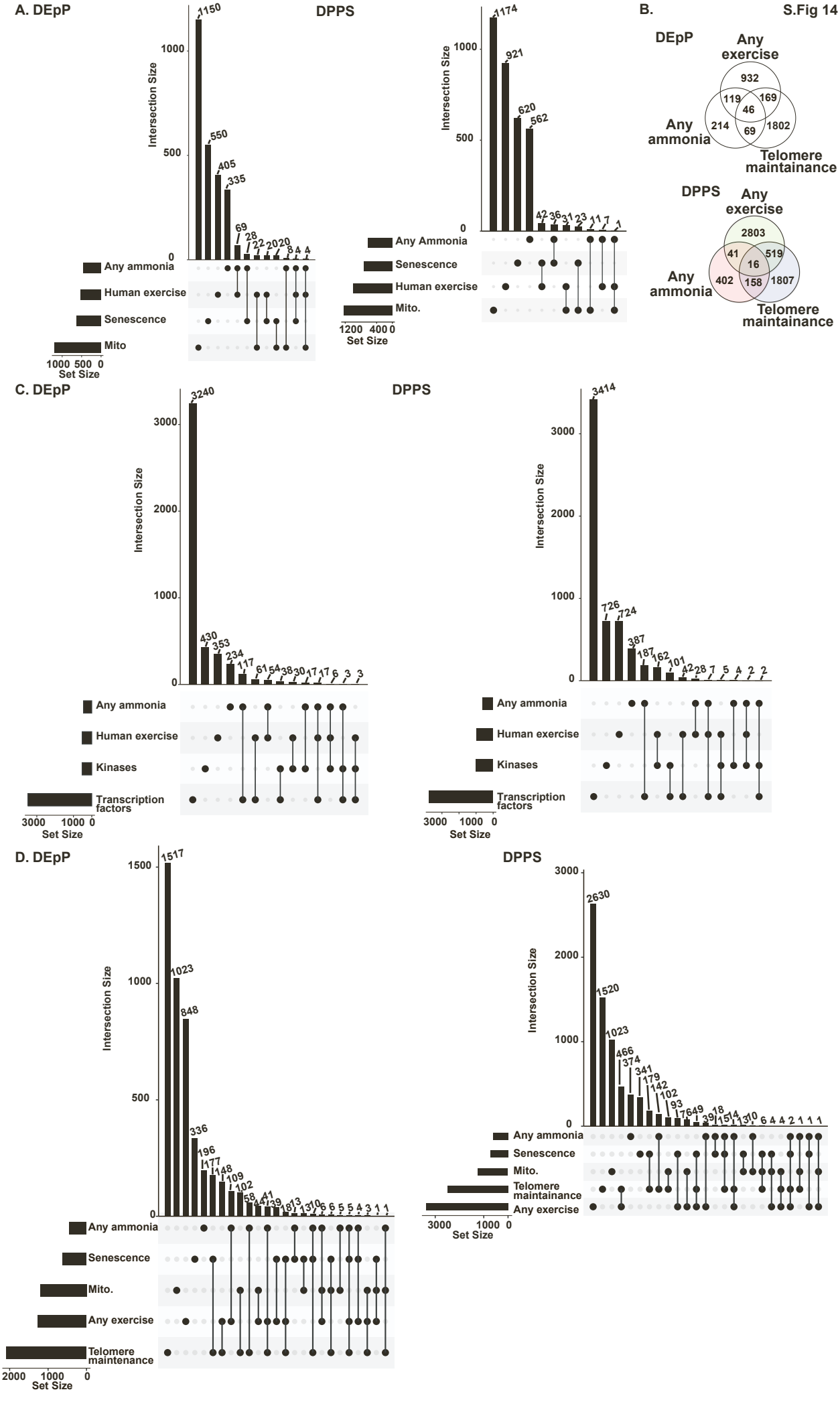
A. DEpP
DPPS
B.
S.Fig 14
Intersection Size
Set Size
Any ammonia
Human exercise
Senescence
Mito
Any Ammonia
Mito.
DEpP
Any exercise
Any ammonia
Telomere maintainance
932
119
169
46
214
69
1802
DPPS
2803
41
519
16
402
158
1807
C. DEpP
DPPS
Kinases
Transcription factors
D. DEpP
DPPS
Any exercise
Telomere maintenance

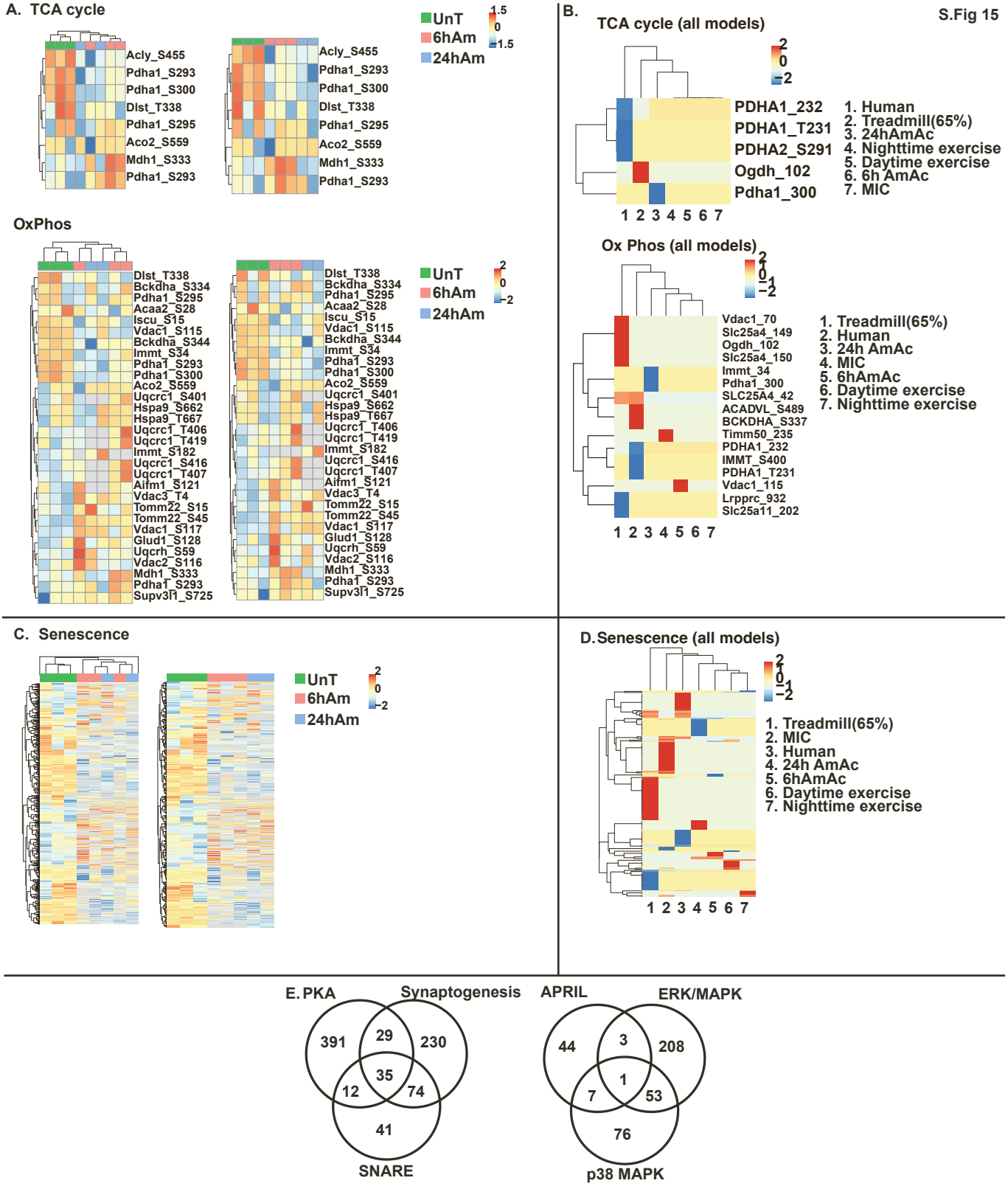
A. TCA cycle
Acly_S455
Pdha1_S293
Pdha1_S300
Dlst_T338
Pdha1_S295
Aco2_S559
Mdh1_S333
Pdha1_S293
UnT
6hAm
24hAm
1.5
0
−1.5
OxPhos
Dlst_T338
Bckdha_S334
Pdha1_S295
Acaa2_S28
Iscu_S15
Vdac1_S115
Bckdha_S344
Immt_S34
Pdha1_S293
Pdha1_S300
Aco2_S559
Uqcrc1_S401
Hspa9_S662
Hspa9_T667
Uqcrc1_T406
Uqcrc1_T419
Immt_S182
Uqcrc1_S416
Uqcrc1_T407
Aifm1_S121
Vdac3_T4
Tomm22_S15
Tomm22_S45
Vdac1_S117
Glud1_S128
Uqcrh_S59
Vdac2_S116
Mdh1_S333
Pdha1_S293
Supv3l1_S725
UnT
6hAm
24hAm
2
0
−2
B.
TCA cycle (all models)
PDHA1_232
PDHA1_T231
PDHA2_S291
Ogdh_102
Pdha1_300
1 2 3 4 5 6 7
1. Human
2. Treadmill(65%)
3. 24hAmAc
4. Nighttime exercise
5. Daytime exercise
6. 6h AmAc
7. MIC
Ox Phos (all models)
Vdac1_70
Slc25a4_149
Ogdh_102
Slc25a4_150
Immt_34
Pdha1_300
SLC25A4_42
ACADVL_S489
BCKDHA_S337
Timm50_235
PDHA1_232
IMMT_S400
PDHA1_T231
Vdac1_115
Lrpprc_932
Slc25a11_202
1 2 3 4 5 6 7
1. Treadmill(65%)
2. Human
3. 24h AmAc
4. MIC
5. 6hAmAc
6. Daytime exercise
7. Nighttime exercise
C. Senescence
UnT
6hAm
24hAm
2
0
−2
D. Senescence (all models)
1 2 3 4 5 6 7
1. Treadmill(65%)
2. MIC
3. Human
4. 24h AmAc
5. 6hAmAc
6. Daytime exercise
7. Nighttime exercise
E. PKA
Synaptogenesis
SNARE
391
29
230
35
12
74
41
APRIL
ERK/MAPK
p38 MAPK
44
3
208
1
7
53
76

S. Fig 16

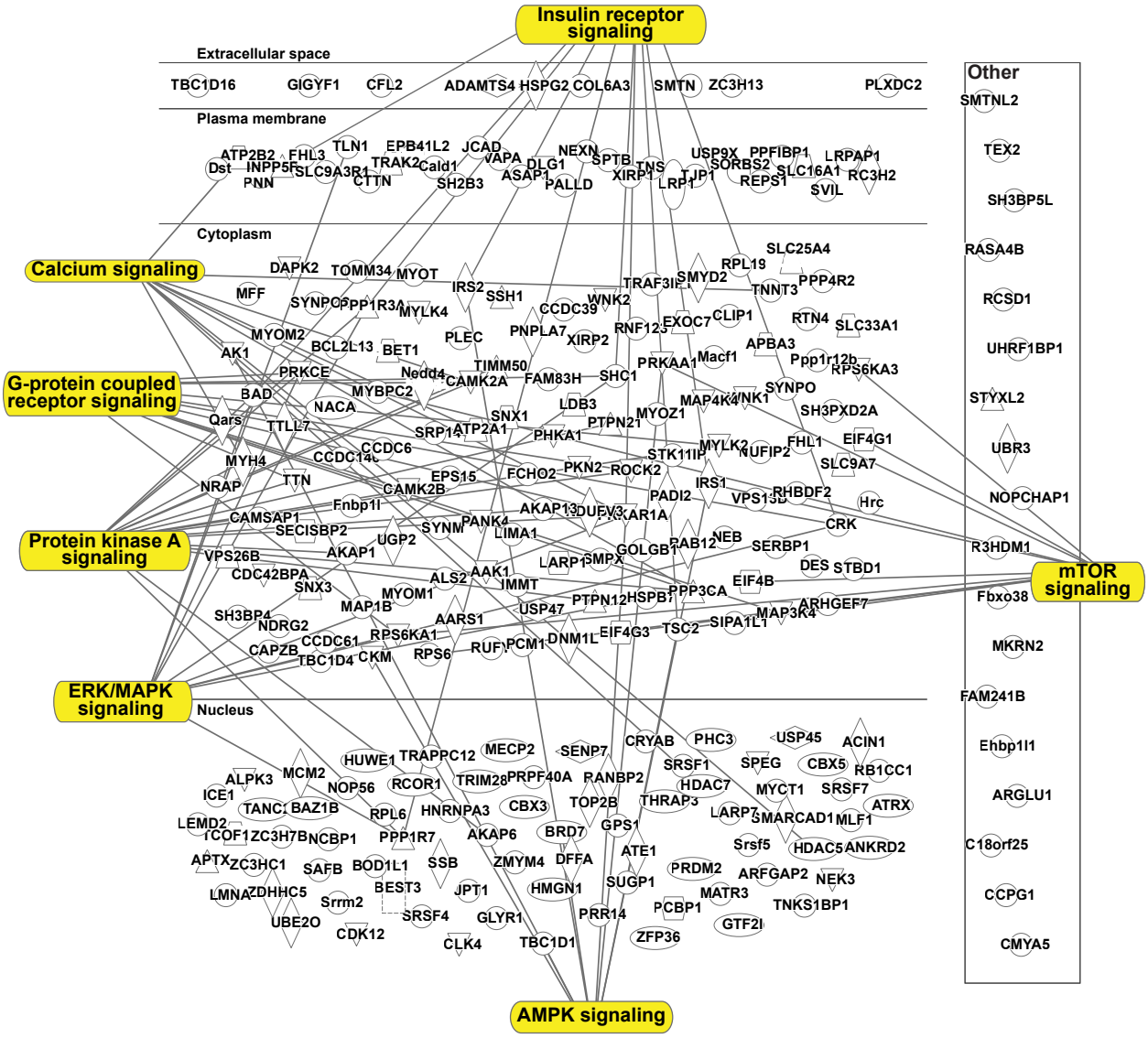
Insulin receptor signaling
Extracellular space
TBC1D16
GIGYF1
CFL2
ADAMTS4
HSPG2
COL6A3
SMTN
ZC3H13
PLXDC2
Plasma membrane
ATP2B2
Dst
INPP5F
PNN
FHL3
SLC9A3R1
TLN1
TRAK2
EPB41L2
CTTN
Cald1
JCAD
SH2B3
VAPA
ASAP1
DLG1
PALLD
NEXN
SPTB
XIRP1
TNS
LRP1
TJP1
USP9X
SORBS2
REPS1
PPFIBP1
SLC16A1
SVIL
LRPAP1
RC3H2
Cytoplasm
Calcium signaling
DAPK2
MFF
TOMM34
MYOT
SYNPO2
PPP1R3A
MYLK4
IRS2
SSH1
WNK2
CCDC39
TRAF3IP1
SMYD2
RPL19
SLC25A4
TNNT3
PPP4R2
EXOC7
CLIP1
RTN4
SLC33A1
MYOM2
AK1
BCL2L13
BET1
PLEC
PNPLA7
XIRP2
RNF123
APBA3
Macf1
PRKAA1
Ppp1r12b
RPS6KA3
G-protein coupled receptor signaling
PRKCE
Nedd4
TIMM50
CAMK2A
FAM83H
SHC1
SYNPO
BAD
MYBPC2
NACA
Qars
TTLL7
SNX1
LDB3
MAP4K4
NK1
MYOZ1
PTPN21
SH3PXD2A
SRP1
ATP2A1
PHKA1
CCDC6
CCDC14
MYH4
TTN
NRAP
EPS15
FCHO2
PKN2
ROCK2
STK11IP
MYLK2
NUFIP2
FHL1
EIF4G1
SLC9A7
CAMK2B
IRS1
PADI2
VPS13B
RHBDF2
Hrc
Fnbp1l
CAMSAP1
SECISBP2
AKAP13
DUFV3
AR1A
CRK
Protein kinase A signaling
UGP2
SYNM
PANK4
LIMA1
AKAP1
VPS26B
CDC42BPA
SNX3
MYOM1
MAP1B
ALS2
AAK1
IMMT
LARP1
SMPX
GOLGB1
PAB12
NEB
SERBP1
DES
STBD1
EIF4B
PPP3CA
PTPN12
HSPB1
USP47
AARS1
RPS6KA1
CCDC61
CAPZB
TBC1D4
CKM
RPS6
RUFY1
PCM1
DNM1L
EIF4G3
TSC2
SIPA1L1
MAP3K4
ARHGEF7
SH3BP4
NDRG2
mTOR signaling
ERK/MAPK signaling
Nucleus
HUWE1
TRAPPC12
MECP2
SENP7
CRYAB
PHC3
USP45
ACIN1
SRSF1
SPEG
CBX5
RB1CC1
ALPK3
MCM2
NOP56
RCOR1
TRIM28
PRPF40A
RANBP2
HDAC7
MYCT1
SRSF7
ICE1
TANC1
BAZ1B
RPL6
HNRNPA3
CBX3
TOP2B
THRAP3
LARP7
SMARCAD1
MLF1
ATRX
LEMD2
TCOF1
ZC3H7B
NCBP1
PPP1R7
AKAP6
BRD7
GPS1
Srsf5
HDAC5
ANKRD2
APTX
ZC3HC1
SAFB
BOD1L1
SSB
ZMYM4
DFFA
ATE1
PRDM2
ARFGAP2
NEK3
LMNA
ZDHHC5
Srrm2
BEST3
JPT1
HMGN1
SUGP1
MATR3
TNKS1BP1
UBE2O
SRSF4
GLYR1
PRR14
PCBP1
GTF2I
CDK12
CLK4
TBC1D1
ZFP36
AMPK signaling
Other
SMTNL2
TEX2
SH3BP5L
RASA4B
RCSD1
UHRF1BP1
STYXL2
UBR3
NOPCHAP1
R3HDM1
Fbxo38
MKRN2
FAM241B
Ehbp1l1
ARGLU1
C18orf25
CCPG1
CMYA5

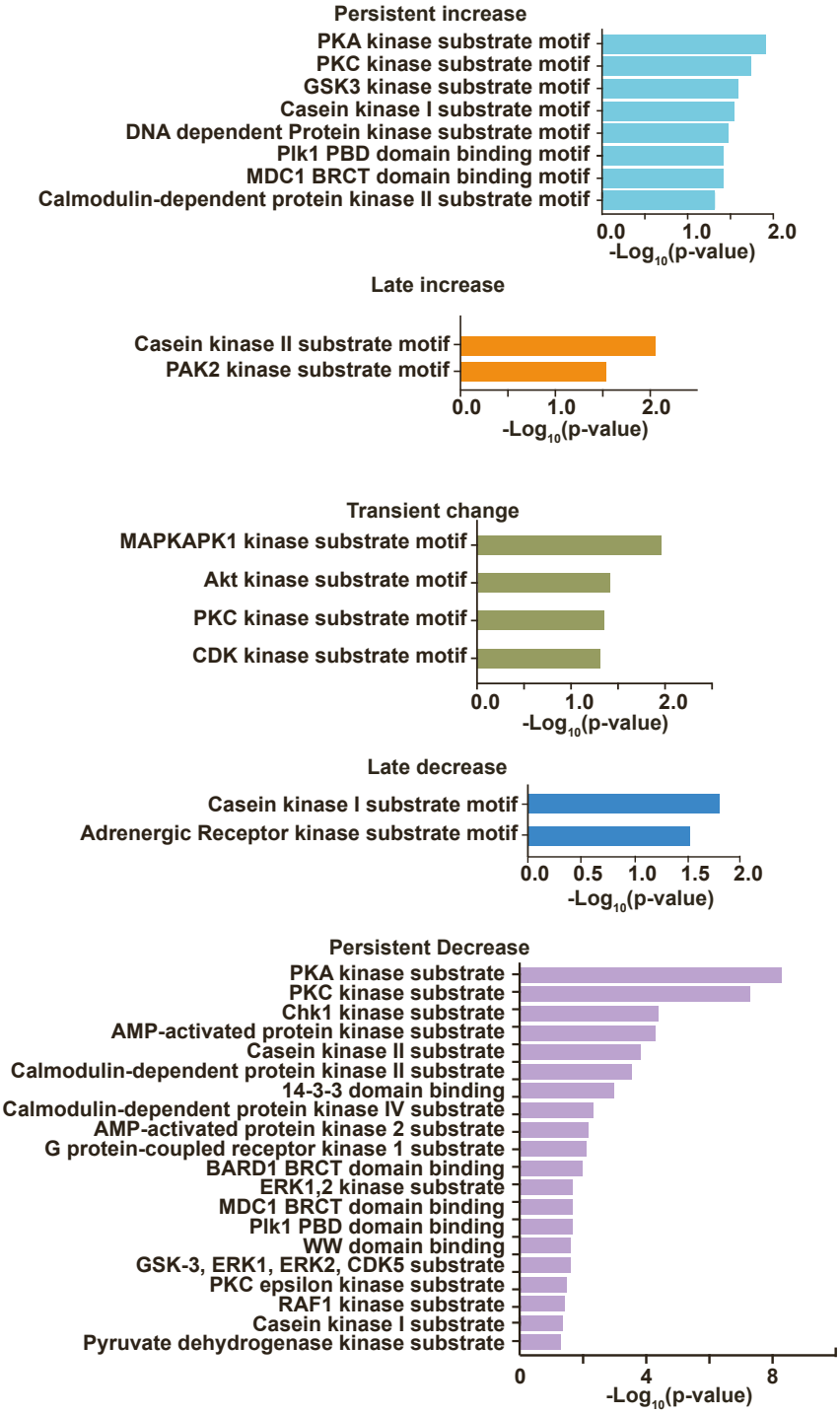
Persistent increase
PKA kinase substrate motif
PKC kinase substrate motif
GSK3 kinase substrate motif
Casein kinase I substrate motif
DNA dependent Protein kinase substrate motif
Plk1 PBD domain binding motif
MDC1 BRCT domain binding motif
Calmodulin-dependent protein kinase II substrate motif
0.0
1.0
2.0
-Log10(p-value)
Late increase
Casein kinase II substrate motif
PAK2 kinase substrate motif
0.0
1.0
2.0
-Log10(p-value)
Transient change
MAPKAPK1 kinase substrate motif
Akt kinase substrate motif
PKC kinase substrate motif
CDK kinase substrate motif
0.0
1.0
2.0
-Log10(p-value)
Late decrease
Casein kinase I substrate motif
Adrenergic Receptor kinase substrate motif
0.0
0.5
1.0
1.5
2.0
-Log10(p-value)
Persistent Decrease
PKA kinase substrate
PKC kinase substrate
Chk1 kinase substrate
AMP-activated protein kinase substrate
Casein kinase II substrate
Calmodulin-dependent protein kinase II substrate
14-3-3 domain binding
Calmodulin-dependent protein kinase IV substrate
AMP-activated protein kinase 2 substrate
G protein-coupled receptor kinase 1 substrate
BARD1 BRCT domain binding
ERK1,2 kinase substrate
MDC1 BRCT domain binding
Plk1 PBD domain binding
WW domain binding
GSK-3, ERK1, ERK2, CDK5 substrate
PKC epsilon kinase substrate
RAF1 kinase substrate
Casein kinase I substrate
Pyruvate dehydrogenase kinase substrate
0
4
8
-Log10(p-value)

A.

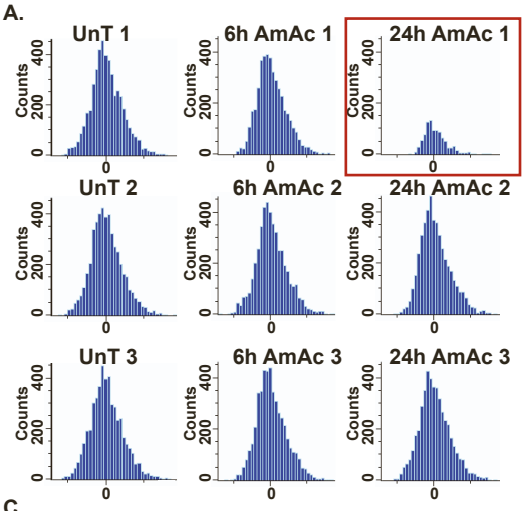

B.

C2C12 myotube biological replicate	Identified phosphosites
UnT 1	5086
6hAmAc 1	4541
24hAmAc 1	1026
UnT 2	5121
6hAmAc 2	5030
24hAmAc 2	5101
UnT 3	5260
6hAmAc 3	5177
24hAmAc 3	5179

C.

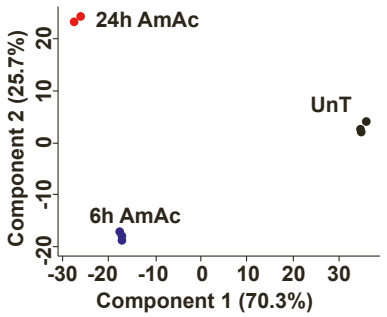

D.

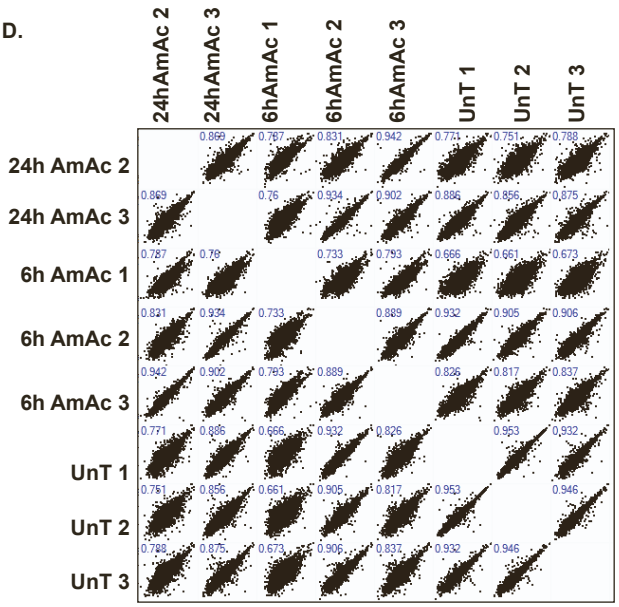

E.

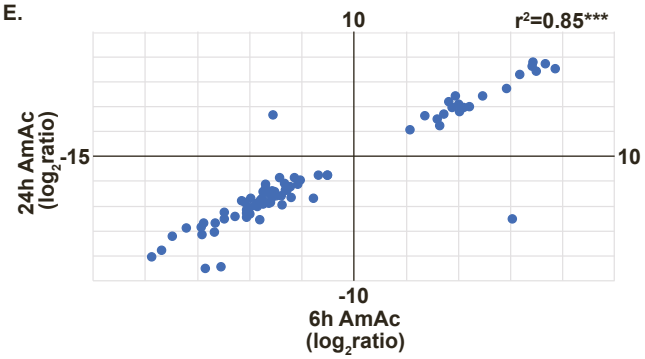

Supplementary Figure Legends

S.Fig 1. Most significant protein networks in the hyperammonemic datasets showed connections to PKA pathway proteins, related to Fig.1. Differentially expressed phosphoproteins (DEpP) were identified in C2C12 myotubes treated with 10mM ammonium acetate (AmAc) for 6h and 24h. Interaction networks were generated from the DEpP followed by feature extraction to include molecules connected to protein kinase A within each dataset. All myotube experiments were done in n=3 biological replicates (one 24hAmAc replicate was removed from downstream analyses due to outlier status). Statistical significance cutoff for DEpP was padj<0.05 (Student's t-test with Benjamini-Hotchberg correction). Red color = increased phosphorylation compared to untreated. Green color = decreased phosphorylation compared to untreated controls.

S.Fig 2. Comparison between untargeted proteomics and phosphoproteomics data in hyperammonemic myotubes, related to Fig.1. **A**. Scatterplot of phosphoprotein expression data compared to proteomics expression data from the same protein in C2C12 myotubes treated with 24h 10mM ammonium acetate (AmAc). **B.** Venn diagram of unique and shared phosphoproteins and proteins, correlation bar graph showing direction of expression change vs control (positive vs. negative) for each shared protein/phosphoprotein that is differentially expressed at 24hAmAc in myotubes, and enriched pathways in differentially expressed phosphoproteins (DEpP) that are not regulated at the protein level and differentially expressed proteins (DEP) that are not regulated at the phosphorylation level. All experiments were done in n=3 biological replicates (one 24hAmAc replicate was removed from downstream analyses due to outlier status). Statistical significance cutoffs were p adj<0.05 for phosphoproteomics and p<0.05 for proteomics to allow for similar numbers of differentially expressed molecules (vs untreated controls). NS= not significant.

S.Fig 3. Phosphoproteomic landscape during hyperammonemia, related to Fig.2. A-C. Pathway enrichment using IPA and DAVID, and heatmaps of the most enriched DAVID functional annotation clusters identified in the differentially expressed phosphoproteins (DEpP) unique to 6h ammonium acetate (AmAc) treatment, unique to 24hAmAc or those shared between 6hAmAc and 24hAmAc phosphoproteomics datasets in C2C12 myotubes. All experiments were done in n=3 biological replicates (one 24hAmAc replicate was removed from downstream analyses due to outlier status). Statistical significance cutoff for full datasets using

IPA was performed using both log_2ratio>|2.5| and padj<0.05 (Student's t-test with Benjamini-Hotchberg false discovery rate correction (BH-FDR)). Foreground DEpP in DAVID analyses was padj<0.05. IPA pathway significance cutoff was the default -log(p-value) $\geq$ 1.3. Perseus 1D analysis significance cutoff was the default BH-FDR>0.02. Green color = DEpP identified in the data subset, Black color = DEpP not identified in the data subset.

S.Fig 4. PKA signaling is altered by various molecules across molecular layers in C2C12 myotubes and in skeletal muscle, related to Fig.2. A. Heatmap showing protein kinase A (PKA) pathway genes that were differentially expressed during 6h and 24h of hyperammonemia (Am) in myotubes (vs. untreated; UnT) in assay for transposase accessible chromatin (ATACseq); and in transcriptomics and proteomics in hyperammonemic myotubes, mice (vs. phosphate buffered saline (PBS)-treated control mice) and human patients with cirrhosis (CIR) (vs healthy subjects (CTL)). **B**. Heatmap of PKA pathway differentially expressed phosphoproteins (DEpP). **C**. Unsupervised and supervised heatmaps showing phosphosite expression in untreated (UnT) myotubes and 6h and 24hAm myotubes in the PKA pathway. All experiments were done in n=3 biological replicates (one 24hAmAc replicate was removed from downstream analyses due to outlier status). Statistical significance cutoff for differentially expressed molecules was performed using the following statistical cutoffs: for ATACseq p<0.005; RNAseq and phosphoproteomics in cells p adj<0.05; proteomics in cells and tissue, and RNAseq in tissue p<0.05 ((Student's t-test with or without Benjamini-Hotchberg false discovery rate correction.

S.Fig 5. Phosphoproteins identified within highly enriched pathways, related to Fig.2. A,B. Unsupervised and supervised heatmaps showing phosphosite expression in myotubes treated with 6h and 24h of ammonium acetate (AmAc) that are components of cyclin dependent kinase, and polo-like kinase (PLK) signaling during 6h and 24h hyperammonemia in myotubes. **C**. Correlation matrix and interaction network of DPPS in the hyperammonemic (6h and 24h) datasets that were components of either PKA signaling or PLK signaling (Numbers show the phosphosite; #1 refers to PKA and #2 refers to PLK. **D**,**E**. Unsupervised and supervised heatmaps showing phosphosite expression in myotubes treated with 6h and 24h of ammonium acetate (AmAc) that are components of HIPPO signaling and hypoxia inducible factor 1α during 6h and 24h hyperammonemia

in myotubes. All myotube experiments were done in n=3 biological replicates (one 24hAmAc replicate was removed from downstream analyses due to outlier status). Statistical significance cutoffs were p adj <0.05 for the differentially phosphorylated phosphosites. Numbers next to gene names refer to the phosphorylated residue within the mouse protein.

S.Fig 6. Venn diagrams comparing molecules identified in critical signaling pathways in myotubes, related to Fig.3. Venn diagram identifying unique and shared molecules across the protein kinase A (PKA), synaptogenesis, synaptic long-term potentiation, insulin receptor signaling in the Ingenuity Pathway Knowledge Database.

S.Fig 7. Enriched GO, KEGG, and Uniprot processes within hyperammonemic myotube phosphoproteomics clusters, related to Fig.3. Differentially phosphorylated phosphosites (DPPS) in C2C12 myotubes treated with 6h and 24h ammonium acetate (AmAc) compared to controls were identified and clustered according to their temporal pattern of change**.** Uniprot (UP) keywords, UP sequence (seq) features, Gene ontology biological processes (GO:BP), molecular functions (GO:MF), cellular components (GO:CC) and Kyoto Encyclopedia of Genes and Genomes (KEGG) pathways enriched in the **A**. Persistent increase (increased phosphorylation at both 6h and 24hAmAc compared to controls), **B**. Late increase (increased phosphorylation only at 24hAmAc compared to controls) clusters of DPPS. **C**. Late decrease (decreased phosphorylation only at 24hAmAc compared to controls) cluster of DPPS. **D.** Transient change (significant change in phosphorylation at 6hAmAc compared to controls but no difference between 24hAmAc treatment and control levels of phosphorylation) and **E**. Persistent decrease (decreased phosphorylation at both 6h and 24hAmAc compared to controls) clusters of DPPS. All experiments were done in n=3 biological replicates (one 24hAmAc replicate was removed from downstream analyses due to outlier status). Statistical significance cutoff for DPPS was padj<0.05 (Student's t-test with Benjamini-Hotchberg correction).

S.Fig 8. Scatterplots correlating mouse exercise phosphoproteomics datasets, related to Fig.4. Scatterplots, linear regressions, and Venn diagrams comparing differentially phosphorylated phosphosites (DPPS) expression (log_2 ratio) from published mouse exercise skeletal muscle phosphoproteomics datasets.

Statistical significance cutoff for DPPS was padj<0.05 (Student's t-test with Benjamini-Hotchberg correction). MIC= maximal (max.) intensity contraction, Treadmill (65% max.) exercise = mice exercised at 65% of their max. running speed on a treadmill, Daytime exercise = mice that underwent high-intensity treadmill running during the zeitgeber time (ZT)0 period of "lights on", Nighttime exercise = mice that underwent high-intensity treadmill running during the ZT12 period of "lights off". p<0.05; *** p<0.001

S.Fig. 9. Shared differentially expressed phosphosites during exercise showed unique and shared pathway responses, related to Fig.4. A. Heat maps showing skeletal muscle DPPS shared in all mouse models and shared within the male mouse models of exercise. **B**. Gene heatmaps of enriched pathways within the exercise datasets. Red is an increased expression and green is decreased expression related to respective controls. Duplicate DEpP were resolved using the greatest absolute value log_2ratio. Numbers next to gene names refer to the phosphorylated residue within the mouse protein. MIC= maximal (max.) intensity contraction, Treadmill (65% max.) exercise = mice exercised at 65% of their max. running speed on a treadmill, Daytime exercise = mice that underwent high-intensity treadmill running during the zeitgeber time (ZT)0 period of "lights on", Nighttime exercise = mice that underwent high-intensity treadmill running during the ZT12 period of "lights off".

S.Fig 10. Regulatory interaction of protein kinase A components in the exercise and hyperammonemia datasets, related to Fig.5. **A**. Unsupervised and supervised heatmaps of phosphosite expression of A-kinase anchoring proteins (AKAP) in myotubes treated with 6h and 24h of ammonium acetate (AmAc)**. B.** Heatmap of differentially phosphorylated phosphosites (DPPS) of AKAP across all datasets. **C**. Heatmap of enriched canonical pathways in each dataset from the subset of DEpP that are shared between at least one hyperammonemia dataset and at least one exercise dataset. **D**. Temporal analysis of enriched processes in DEpP at 6h and 24h AmAc with shared DEpP from any exercise dataset. All myotube experiments were done in n=3 biological replicates (one 24hAmAc replicate was removed from downstream analyses due to outlier status). DEpP/DPPS was padj<0.05 (Student's t-test with Benjamini-Hotchberg correction) for ammonia and mouse data and padj<0.05 and expression fold change >|1.5| for human data. MIC= maximal (max.) intensity contraction, Treadmill (65% max.) exercise = mice exercised at 65% of their max. running speed on a

treadmill, Daytime exercise = mice that underwent high-intensity treadmill running during the zeitgeber time (ZT)0 period of “lights on”, Nighttime exercise = mice that underwent high-intensity treadmill running during the ZT12 period of “lights off”.

S.Fig 11. **Protein-protein interaction networks identified by functional enrichment analysis (STRING) of highly correlated differentially expressed phosphoproteins (DEpP), related to Fig.5.** C2C12 myotubes were treated with 6h and 24h of ammonium acetate (AmAc) and skeletal muscle from models of exercise in mouse and humans. STRING was used to identify interaction networks using known protein-protein interactions between DEpP. All myotube experiments were done in n=3 biological replicates (one 24hAmAc replicate was removed from downstream analyses due to outlier status). DEpP was padj<0.05 (Student’s t-test with Benjamini-Hotchberg correction) for myotube data and padj<0.05 and expression fold change >|1.5| for human data.

S.Fig 12. Unique and shared differentially expressed phosphorylation across hyperammonemia and exercise datasets, related to Fig.5. A. Venn diagram showing differentially expressed phosphoproteins (DEpP) and differentially phosphorylated phosphosites (DPPS) present in at least one of the 6h or 24h ammonium acetate (AmAc)-treated myotube datasets compared to DEpP/DPPS present in at least one of the mouse exercise datasets. **B**. Venn diagram of DEpP and DPPS shared between any AmAc dataset and the human exercise dataset. **C**. Venn diagram of DEpP and DPPS shared between the 6h AmAc dataset , the 24h AmAc dataset, and the human exercise dataset. **D**. Venn diagram of DEpP and DPPS shared between the 6h AmAc dataset , the 24h AmAc dataset, and at least one of the mouse exercise datasets. **E**. Venn diagram of DEpP and DPPS shared between at least one of the hyperammonemia datasets, at least one of the mouse exercise datasets, and the human exercise dataset. **F**. Upset plot showing unique and shared DEpP and DPPS between each phosphoproteomics dataset analyzed. All myotube experiments were done in n=3 biological replicates (one 24hAmAc replicate was removed from downstream analyses due to outlier status). All mouse and human experiments from previously published manuscripts were done in at least n=3 individuals. DEpP/DPPS was padj<0.05 (Student’s t-test with Benjamini-Hotchberg correction) for ammonia and mouse data and padj<0.05 and expression fold change >|1.5| for human data. MIC= maximal (max.)

intensity contraction, Treadmill (65% max.) exercise = mice exercised at 65% of their max. running speed on a treadmill, Daytime exercise = mice that underwent high-intensity treadmill running during the zeitgeber time (ZT)0 period of “lights on”, Nighttime exercise = mice that underwent high-intensity treadmill running during the ZT12 period of “lights off”.

S.Fig 13. Shared DPPS on DEpP across all exercise and hyperammonemia datasets, related to Fig.5. Dot plot showing the expression level (log2ratio) of each differentially phosphorylated phosphosite (DPPS) on shared differentially expressed phosphoprotein (DEpP) in the hyperammonemia phosphoproteomics dataset, the human exercise phosphoproteomics dataset, and the following mouse exercise datasets: nighttime exercise, daytime exercise, treadmill exercise at 65% of maximal (max.) running speed, and max. intensity contractions (MIC) in the skeletal muscle of an anesthetized mouse. All myotube experiments were done in n=3 biological replicates (one 24hAmAc replicate was removed from downstream analyses due to outlier status). DEpP/DPPS was padj<0.05 (Student’s t-test with Benjamini-Hotchberg correction) for ammonia and mouse data and padj<0.05 and expression fold change >|1.5| for human data. Daytime exercise = mice that underwent high-intensity treadmill running during the zeitgeber time (ZT)0 period of “lights on”, Nighttime exercise = mice that underwent high-intensity treadmill running during the ZT12 period of “lights off”.

S.Fig 14. Comparative phosphoproteomics analysis of the unique and overlapping differentially expressed phosphoproteins (DPPS) and differentially phosphorylated phosphosites (DEpP), related to Fig.6. Untargeted phosphoproteomics was performed in C2C12 myotubes with 6h and 24h of ammonium acetate treatment. These data were compared to previously published phosphoproteomics data from muscle from human subjects and mice before and after exercise. **A**. Upset plots showing unique and shared genes between the human exercise DEpP/DPPS dataset, at least one hyperammonemia DEpP/DPPS dataset, a senescence gene database, and a mitochondrial gene database. **B**. Venn diagrams showing unique and shared genes between at least one exercise DPPS dataset, at least one hyperammonemia DEpP/DPPS dataset, and a telomere maintenance gene database. **C**. Upset plots showing unique and shared genes between at least one exercise DEpP/DPPS dataset, at least one hyperammonemia DEpP/DPPS dataset, a kinase database, and a transcription factor database. **D**. Upset plots showing unique and shared genes

between at least one exercise DEpP/DPPS dataset, at least one hyperammonemia DEpP/DPPS dataset, a database of senescence-related genes, a database of mitochondrial genes, and a database of telomere maintenance genes. DEpP/DPPS was padj<0.05 (Student's t-test with Benjamini-Hotchberg correction) for ammonia and mouse data and padj<0.05 and expression fold change >|1.5| for human data. All myotube experiments were done in n=3 biological replicates (one 24hAmAc replicate was removed from downstream analyses due to outlier status). All mouse and human experiments from previously published manuscripts were done in at least n=3 individuals. Mito. = Verified mitochondrial genes from the MitoCarta3.0 database. Any ammonia = DPPS was present in at least one of either the 6h or 24hAmAc datasets. Any exercise = DPPS was present in at least one of the exercise datasets (mice or human).

S.Fig.15. Phosphorylation of mitochondrial and senescence pathway genes, related to Fig.6. **A**. Supervised and unsupervised heatmaps of phosphosite expression of tricarboxylic acid (TCA) cycle and oxidative phosphorylation (OxPhos; electron transport chain) components in myotubes treated with 6h and 24h of ammonium acetate (AmAc)**. B.** Heatmap of differentially phosphorylated phosphosites (DPPS) of TCA cycle and OxPhos. components in myotubes treated with 6h and 24h of ammonium acetate (AmAc) and any exercise dataset. **C**. Supervised and unsupervised heatmaps of phosphosite expression of senescence components in hyperammonemic myotubes. **D**. Heatmap of DPPS of senescence components in myotubes treated with 6h and 24h of AmAc and any exercise dataset. **E**. Venn diagrams identifying unique and shared molecules across the protein kinase A (PKA), synaptogenesis, synaptosome associated protein receptor (SNARE) and APRIL (A proliferation-inducing ligand), extracellular signal regulated kinase (ERK)-mitogen-activated protein kinase (MAPK), and p38 MAPK pathways in the Ingenuity Pathway Analysis Qiagen Knowledgebase.

S.Fig. 16. Connectivity network of multiple levels of interactions and regulation by canonical during exercise and hyperammonemia, related to Fig.7. Motifs were identified for the hyperammonemic, mice and human exercise differentially phosphorylated phosphosites (DPPS) and proteins with protein kinase A (PKA) binding sites were mapped based on canonical pathway enrichments in the Ingenuity Pathway Knowledge Database.

S.Fig 17. Motifs enriched in temporal clusters of differentially phosphorylated phosphosites, related to Fig.7. Persistent increase (increased phosphorylation at 6h and 24h of ammonium acetate (AmAc) treatment compared to controls), Late increase (increased phosphorylation at 24h AmAc compared to controls but no change at 6hAmAc compared to controls), Late decrease (decreased phosphorylation at 24hAmAc compared to controls but not at 6hAmAc compared to controls, Transient change (change in phosphorylation at 6hAmAc and return to control levels of phosphorylation at 24hAmAc), Persistent decrease (decrease in phosphorylation at both 6h and 24hAmAc compared to controls) clusters of differentially phosphorylated phosphosites (DPPS) were analyzed and motifs enriched in each of the five DPPS clusters were identified. All experiments were done in n=3 biological replicates (one 24hAmAc replicate was removed from downstream analyses due to outlier status). Statistical significance cutoff for DPPS was padj<0.05 (Student's t-test with Benjamini-Hotchberg correction).

S.Fig 18. Quality control for C2C12 hyperammonemia phosphoproteomics datasets, related to STAR Methods. A. Read counts for phosphorylated peptides in each dataset. Red box indicates the outlier sample. **B.** Number of phosphorylated peptides identified in each biological replicate and each treatment group for the phosphoproteomics dataset of C2C12 myotubes treated with 10mM ammonium acetate (AmAc) including the outlier sample. **C**. PCA plot for the hyperammonemic myotube phosphoproteomics dataset with outlier sample removed. **D**. Correlation quality control plot for the hyperammonemic phosphoproteomics dataset with outlier sample removed. **E**. Scatterplot comparing shared differentially phosphorylated phosphosites (DPPS) between the 6hAmAc phosphoproteomics dataset and the 24hAmAc phosphoproteomics dataset. All myotube experiments were done in n=3 biological replicates (one 24hAmAc replicate was removed from downstream analyses due to outlier status).

ST1. Index to Supplementary Tables

S.Table Number	Figure supported	Topic
ST1	None	Index to Supplementary Tables, related to STAR Methods
ST2	Fig.1,A-C	AmAc phosphoproteomic landscape, related to Fig.1
ST3	S.Fig.1	AmAc network data, related to Fig.1
ST4	S.Fig.2,A,B	AmAc phosphoproteomics vs proteomics, related to Fig.1
ST5	Fig.2,A,B	AmAc functional enrichment, related to Fig.2
ST6	S.Fig.3,A-C	AmAc pathway and heatmaps, related to Fig.2
ST7	S.Fig.4,A-C	AmAc PKA heatmaps, related to Fig.2
ST8	S.Fig.5,A-E	Highly enriched pathway components, related to Fig.2
ST9	S.Fig.6	Molecules shared between pathways, related to Fig.3
ST10	Fig.3,A-F	Cluster IPA pathways, related to Fig.3
ST11	S.Fig.7,A-E	DAVID annotated hyperammonemia clusters, related to Fig.3
ST12	Fig.4,A-E	Differentially expressed phosphoproteins in exercise datasets, related to Fig.4
ST13	S.Fig.8	Mouse vs. mouse scatter plots and Venns, related to Fig.4
ST14	S.Fig.9,A,B	Exercise heatmaps, related to Fig.4
ST15	Fig.5,A,B,E,F,G,H	AmAc and exercise comparison analyses, related to Fig.5
ST16	S.Fig.10,A-D	AKAP for exercise and AmAc shared DPPS, related to Fig.5
ST17	S.Fig.11	STRING for exercise and AmAc shared DPPS, related to Fig.5
ST18	(text only)	PKA signaling pathway molecules, related to Fig.2
ST19	S.Fig.12,A-F	Venn diagrams comparing DEpP/DPPS in AmAc myotubes and mouse & human skeletal muscle with exercise, related to Fig.5
ST20	S.Fig.13	All phosphosites scatter, related to Fig.5
ST21	Fig.6,A-D	Comparison of AmAc and exercise datasets with verified databases and shared canonical pathways and DPPS, related to Fig.6
ST22	S.Fig.14,A-D	Comparison of DEpP, DPPS to verified databases, related to Fig.6
ST23	S.Fig.15,A-E	Mitochondrial and senescence heatmaps, related to Fig.6
ST24	Fig.7,A-E	Motifs and predicted kinases identified in all datasets, related to Fig.7
ST25	S.Fig.16	Proteins shared in PKA motif prediction, related to Fig.7
ST26	S.Fig.17	Motifs enriched in hyperammonemic clusters, related to Fig.7
ST27	(text only)	Searchable all mouse & human data, related to STAR Methods
ST28	S.Fig.18	Ammonia phosphoproteomics QC, related to STAR Methods

Abbreviations: AKAP: A-kinase anchoring protein, AmAc: Ammonium acetate, DEpP: Differentially expressed phosphoprotein, DPPS: Differentially phosphorylated phosphosite, Fig: Figure, S.Fig: Supplementary figure; ST: Supplementary Table; IPA: Ingenuity Pathway Analysis; PKA: Protein kinase A; QC: Quality control